Soil Dynamics and Earthquake Engineering 124 (2019) 212–229

Contents lists available at ScienceDirect

Soil Dynamics and Earthquake Engineering

journal homepage: www.elsevier.com/locate/soildyn

System response of liquefiable deposits

Misko Cubrinovski[a,*], Aimee Rhodes[b,1], Nikolaos Ntritsos[a], Sjoerd Van Ballegooy[c]

[a] University of Canterbury, Civil and Natural Resources Engineering, Private Bag 4800, Christchurch, New Zealand
[b] WSP Opus, L10 Majestic Centre, 100 Willis St, Wellington, New Zealand
[c] Tonkin + Taylor, Ltd., 105 Carlton Gore Rd, Newmarket, Auckland 1023, New Zealand

ARTICLE INFO

Keywords:
Case history
Earthquake
Effective stress analysis
Liquefaction
System response

ABSTRACT

Detailed geotechnical characterization and in-depth liquefaction assessment using seismic effective stress analyses are presented for 55 liquefaction case histories (sites) from Christchurch. Fifteen of the sites manifested liquefaction in the two major earthquakes during the 2010–2011 Canterbury earthquakes (YY-sites), while 17 sites did not manifest liquefaction in either event (NN-sites). The YY- and NN-sites are shown to have practically identical critical layer characteristics, with low CPT tip resistance (q_{c1Ncs} = 80–86), and shallow location of the critica.l layer at approximately 2 m depth. However, there are significant differences between the YY- and NN-sites with regard to their deposit characteristics including the thickness and vertical continuity of their critical zones and liquefiable materials.

Effective stress analyses are used to demonstrate key mechanisms of system-response of liquefying deposits that either intensify (for the YY-sites) or mitigate (for the NN-sites) liquefaction manifestation at the ground surface. The study illustrates the need to consider system-response of liquefying soils in the assessment of liquefaction manifestation and severity of liquefaction-induced damage.

1. Introduction

Simplified liquefaction triggering procedures used in current engineering practice have been developed based on case histories in which liquefaction was manifested at the ground surface during past earthquakes. Such liquefaction case histories essentially reflect the overall response of soil deposits during earthquakes, and their key characteristics with regard to the severity of liquefaction manifestation. However, despite the intent to capture the overall performance of the deposit at a given site, in the simplified liquefaction evaluation procedures each layer is considered in isolation, and a factor of safety against liquefaction triggering, maximum shear and volumetric strains are estimated separately, and independently, for each layer. In these calculations, interactions between different layers in the dynamic response, and through excess pore water pressures and water flow are ignored. Hence, principal mechanisms of interaction or *system-response* effects of liquefying deposits that potentially contribute to the severity of liquefaction manifestation are not accounted for in the simplified procedures. Liquefaction damage indices, such as *LSN* [22] and *LPI* [14,15] use specific weighting functions to quantify the damage potential of liquefying layers depending on their proximity to the ground surface, but still they do not account for cross-interactions between different layers during the development of liquefaction and post-liquefaction triggering.

In the 2010–2011 Canterbury Earthquake Sequence (CES) widespread and damaging liquefaction affected nearly half of the urban area of Christchurch including 60,000 residential buildings and properties. Particularly severe liquefaction occurred in the eastern suburbs of Christchurch along the Avon River where lateral spreading also occurred [9]. After the 2010–2011 earthquakes, several studies were carried out to scrutinize the accuracy of simplified liquefaction evaluation procedures in predicting liquefaction triggering (manifestation) and associated damage. Green et al. [12] found that the CPT-based procedures of Idriss and Boulanger [13], Robertson and Wride [18] and Moss et al. [16] accurately predicted the liquefaction manifestation for the majority of 25 well-documented case history sites from Christchurch and Kaiapoi. Van Ballegooy et al. [22] and Maurer et al. [15] used the large CPT database in Christchurch to find that liquefaction damage indices such as LSN and LPI were capable of depicting general trends in liquefaction damage, and provided an improved definition and guidance for use of such damage indices. However, they also found that in a significant number of cases predictions from the simplified methods

* Corresponding author.
E-mail addresses: misko.cubrinovski@canterbury.ac.nz (M. Cubrinovski), aimee.rhodes@wsp-opus.co.nz (A. Rhodes), nikolaos.ntritsos@pg.canterbury.ac.nz (N. Ntritsos), SVanBallegooy@tonkintaylor.co.nz (S. Van Ballegooy).
[1] Past address: University of Cantenbury.

https://doi.org/10.1016/j.soildyn.2018.05.013
Received 13 January 2018; Received in revised form 27 April 2018; Accepted 8 May 2018
Available online 21 May 2018
0267-7261/

were inconsistent with field observations.

Initial observations from the 2010–2011 Canterbury earthquakes also indicated that system response of liquefying deposits was a significant factor for both manifestation of liquefaction and severity of liquefaction-induced damage. In the initial screening, clear anomalies were identified in the predictions by the simplified methods. Importantly, biases in the predictions were seen in which systematic over-predictions of liquefaction occurrence or mispredictions were observed in specific areas, and for certain types of soils and stratification of deposits.

This paper explores key differences in the deposits and liquefaction responses of 55 well-documented case histories of level ground free field sites that showed vastly different performance during the earthquakes, from no liquefaction manifestation to extreme severity of liquefaction. The sites are first grouped with regard to their liquefaction manifestation (performance), and a simplified soil profile is developed for each site. Characteristics of the soil profiles at sites that liquefied in the two major earthquakes are comparatively examined with the soil profiles at sites that did not manifest liquefaction in either event. Following the initial geotechnical characterization and analysis, rigorous effective stress analyses were performed to identify key mechanisms that led to the vastly different performances for the two types of sites. This paper demonstrates the important effects of system response of liquefiable deposits and the need to incorporate these effects in the assessment of liquefaction and associated damage.

2. Investigated Christchurch sites

2.1. Liquefaction manifestation

In the period between September 2010 and December 2011, a series of strong earthquakes occurred in the Canterbury region (New Zealand). Four of these earthquakes caused a significant seismic demand and liquefaction-induced damage in the urban area of Christchurch. The first in the sequence was the 4 September 2010 M_w7.1 earthquake (Darfield earthquake), which caused peak ground accelerations of about 0.20*g* in most of Christchurch, and severe liquefaction and lateral spreading along the Avon River [6,8]. Fig. 1a shows areas of liquefaction-induced land damage in the 4SEP2010 earthquake, where solid symbols indicate the locations of the 55 sites, which are the subject of this study. An equivalent liquefaction-induced land damage map for the most destructive 22 February 2011 M_w6.2 earthquake (Christchurch earthquake) is shown in Fig. 1b. As the source of this event was practically within the city boundaries (along the southeast perimeter of the city), it generated more severe ground motions and triggered more extensive liquefaction in the eastern suburbs of Christchurch. In this event, the peak ground accelerations were generally in the range from 0.35*g* to 0.55*g* in the areas affected by widespread liquefaction. Again, the most severe liquefaction and lateral spreading were manifested along the Avon River [7,9].

At each of the 55 sites, detailed assessment of land damage was conducted by Tonkin&Taylor engineers using field inspections, observations from aerial photography, and estimates of settlement (subsidence) based on pre- and post-earthquake LiDAR surveys. The severity of liquefaction at sites that manifested liquefaction was classified as: moderate, major, severe and very severe, based on the classification adopted by Russell and van Ballegooy [19]. Hence, the performance of the sites during these two earthquakes varied from no liquefaction manifestation at the ground surface to very severe liquefaction, in which case a large area of the site was covered by thick soil ejecta.

Based on the observed liquefaction manifestation, the 55 sites were classified into three groups: (i) sites that manifested liquefaction (soil ejecta) in both 4 September 2010 and 22 February 2011 earthquakes (YY-cases, shown with red symbols in Fig. 1); (ii) sites that did not manifest liquefaction in the September event but manifested liquefaction in the 22 February 2011 earthquake (NY-cases; black symbols in Fig. 1); and, (iii) sites that did not manifest liquefaction in either event (NN-cases; green symbols in Fig. 1). Table 1 summarizes the liquefaction manifestation for the 55 sites.

Most of the sites (32 of 38 sites) that liquefied in the February 2011 earthquake did manifest liquefaction in the subsequent M_w6.0 13 June 2011 event, and some of these sites also re-liquefied during the last in the sequence M_w5.9 23 December 2011 earthquake. To eliminate some of the complexities associated with re-liquefaction, in this study we focus on the performance of the sites during the first two events. It is worth emphasizing that the 17 NN-sites did not manifest liquefaction, in any event, during the CES (2010–2011 earthquakes).

2.2. Geotechnical characterization

Detailed field investigations were performed at each site including CPT and high-resolution (at 200 mm intervals) compression wave and shear wave velocity (V_p and V_s respectively) measurements using direct-push cross-hole technique [3]. The V_p profiles were used as a principal indicator for the level of saturation throughout the depth of the deposits in conjunction with detailed groundwater table model for Christchurch [21,23]. A large number of disturbed samples were recovered from target soils/layers for index testing in the laboratory to determine the grain-size distribution, fines content and plasticity of fines. At each of the 55 sites, borehole data was also available from previous investigations, at a close but non-intrusive distance from the locations of CPT and cross-hole testing.

Here, an attempt is presented to characterize the sites using predominantly the CPT data, and then examine similarities and differences between soil profiles that exhibited liquefaction in both earthquakes (YY-cases) and those sites where no liquefaction manifestation was observed in either event (NN-cases). The intermediate NY-cases involve additional complexities in the interpretation, and therefore were left out from this initial study and will be presented in follow-on publications.

There were several objectives in mind when developing the methodology for geotechnical characterization of the 55 sites. First, it was intended to develop representative soil profiles for each liquefaction manifestation group (i.e. YY-, NY-, and NN-sites), in which soil types, soil density (penetration resistance), thickness and sequence of layers will be characterized. Importantly, the representative soil profiles should allow for comparison of characteristics of identified critical layers, and the deposit as a whole, between the YY- and NN- profiles. Finally, the representative profiles should provide basis for their rigorous modelling using seismic effective stress analyses in order to explore key mechanisms and processes that either intensify or mitigate liquefaction manifestation at the ground surface. With these objectives in mind, the simplified deterministic methodology presented below was developed first; more robust approach including probabilistic treatment of uncertainties is currently under way for characterization of the 55 sites.

2.3. Simplified soil profiles

Using the CPT data, simplified soil profiles were determined for each of the 55 sites. The approach was to first identify depth intervals over which the cone tip resistance (q_c) and the soil behaviour type index (I_c) can be approximated by constant values, as illustrated in Fig. 2 for an Avondale site. On this basis, soil layers were defined, as shown with the leftmost soil-column in Fig. 2. The layers were then classified based on the I_c-value into soil behaviour type associated with: coarse sands and gravelly soils ($I_c \leq 1.3$); clean sands ($1.3 < I_c \leq 1.8$); sands with small amount of fines ($1.8 < I_c \leq 2.1$); sandy silts and non-plastic silts ($2.1 < I_c \leq 2.6$); non-liquefiable silt/clayey/peat soils ($I_c > 2.6$). The particular boundaries separating between fine sands and fines-containing sands ($I_c = 1.8$) and fines-containing sands and non-plastic silts ($I_c = 2.1$) are approximate, but appropriate thresholds based on our

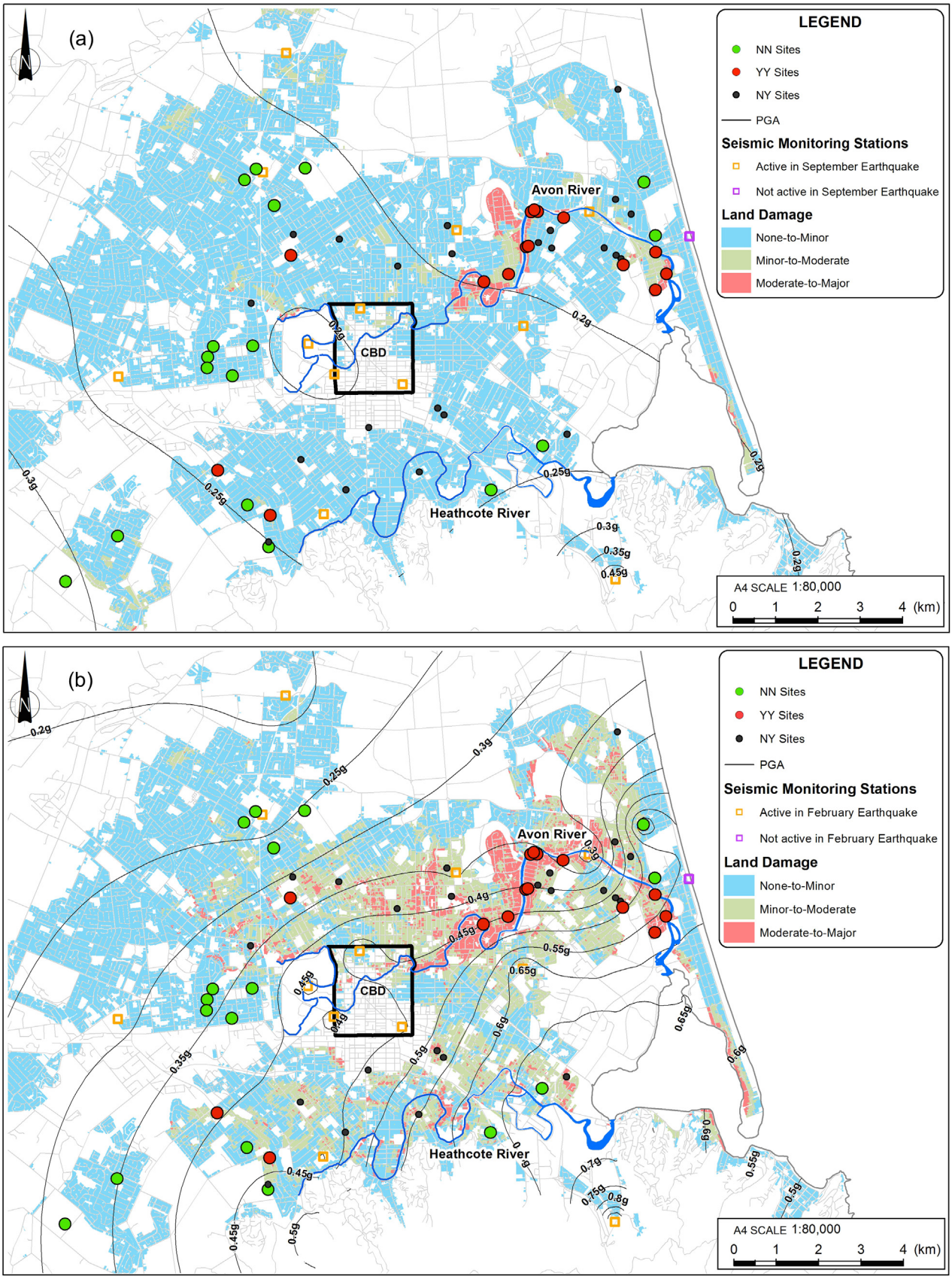

Fig. 1. Locations of 55 investigated sites (circular symbols) and land damage caused by soil liquefaction (background colours) in: (a) 4 September 2010 earthquake; (b) 22 February 2011 earthquake (base maps reproduced from [19]). (For interpretation of the references to color in this figure legend, the reader is referred to the web version of this article.).

Table 1
Summary of liquefaction manifestation at the 55 sites during the 4 September 2010 and 22 February 2011 Canterbury Earthquakes.

Earthquake	Liquefaction manifestation		
	YY (15 sites)	NY (23 sites)	NN (17 sites)
4SEP2010	Yes	No	No
22FEB2011[a]	Yes	Yes	No

[a] Imposed the highest seismic demand across the city, except for the north-west part (3–4 sites) and south-west part (2 sites).

current understanding of Christchurch soils and their associated I_c values. The water table was defined at each site based on the detailed groundwater model for Christchurch [23]. In many cases, the water table is shallow at 1.5–2 m depth.

The leftmost soil-column plot in Fig. 2 depicts the characteristic layering for the profile. For each layer, q_c and I_c values are defined, thus characterizing both the soil behaviour type and penetration resistance of the layer. In the layering definition, visual classification based on borehole data was used as supporting information.

Clearly, the simplified q_c and I_c profiles (solid red lines) deviate more or less from the original irregular q_c and I_c traces (black lines). To verify that these differences due to the profile simplification are not significantly affecting the outcomes from simplified liquefaction evaluation procedures, triggering analyses and subsequent settlement calculations were carried out for each site using both the simplified profiles and the original q_c and I_c traces. These analyses confirmed that, for all practical purposes, the simplified profiles yield identical outcomes to those obtained from triggering and settlement analyses using the original q_c and I_c traces. In other words, the computed factors of safety, depth of liquefaction and associated settlement for the simplified profiles were fully consistent with the respective results obtained using the original profiles.

2.4. Critical layers

Current semi-empirical liquefaction triggering procedures have been developed based on case histories of liquefaction manifestation in which *CSR*-q_c pairs (in the case of CPT-based procedures) were identified for each case history (site). The *CSR*-q_c pairs at each site represent the values of the seismic demand (load) and penetration resistance for the critical layer that was considered *responsible* for the liquefaction manifestation at the site. In effect, the critical layer can be seen as the layer that is the most likely to trigger and manifest liquefaction at the ground surface of a given site.

With this background in mind, triggering analyses were performed for the 4 September 2010 and 22 February 2011 earthquakes, for all 55

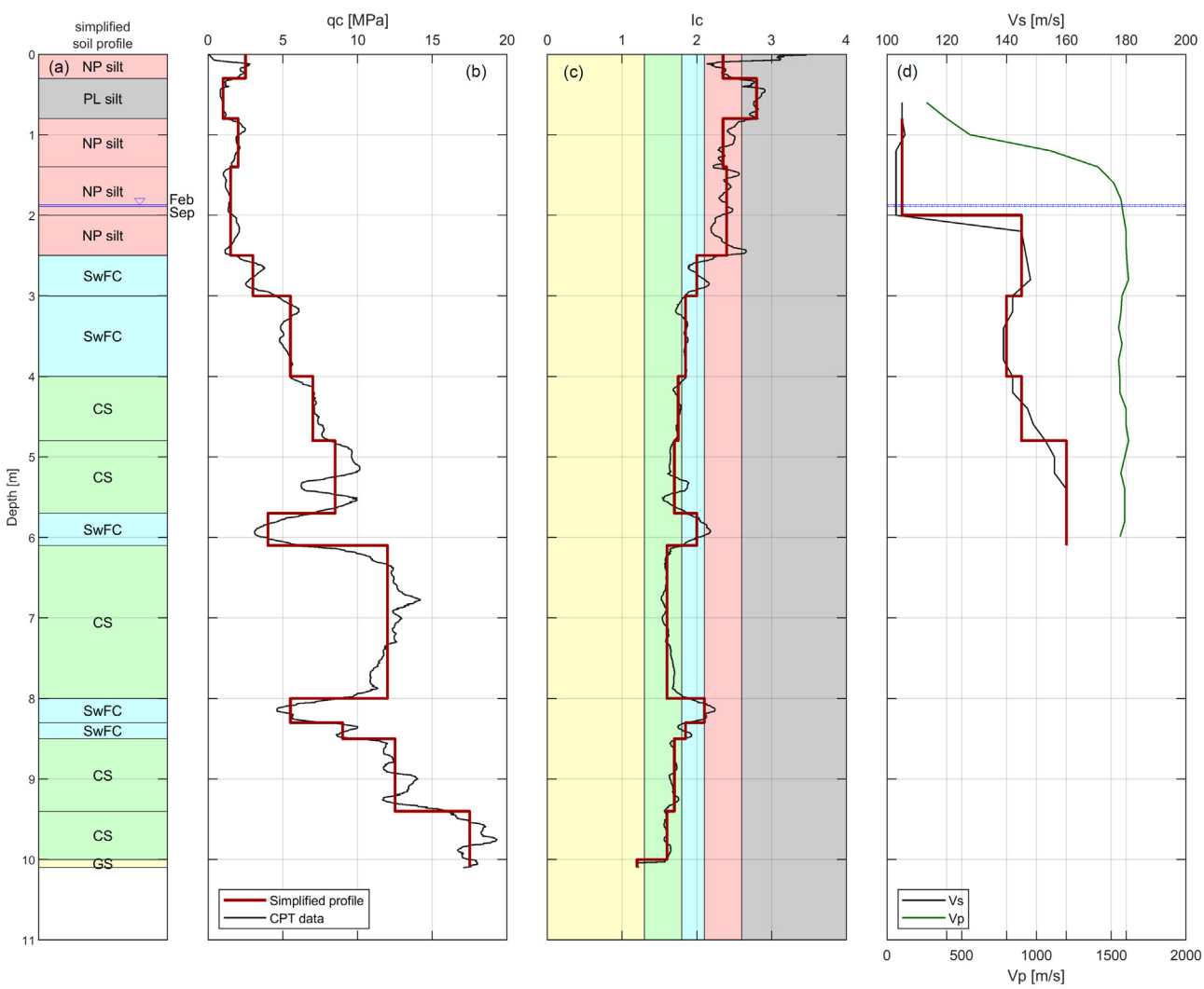

Fig. 2. Determination of a simplified soil profile for an Avondale site [17]: (a) simplified soil profile (stratification); (b) q_c values; (c) I_c values; (d) V_s and V_p profiles; *irregular black lines show original q_c and I_c traces; solid straight red lines indicate values used in the simplified profile.* (For interpretation of the references to color in this figure legend, the reader is referred to the web version of this article.).

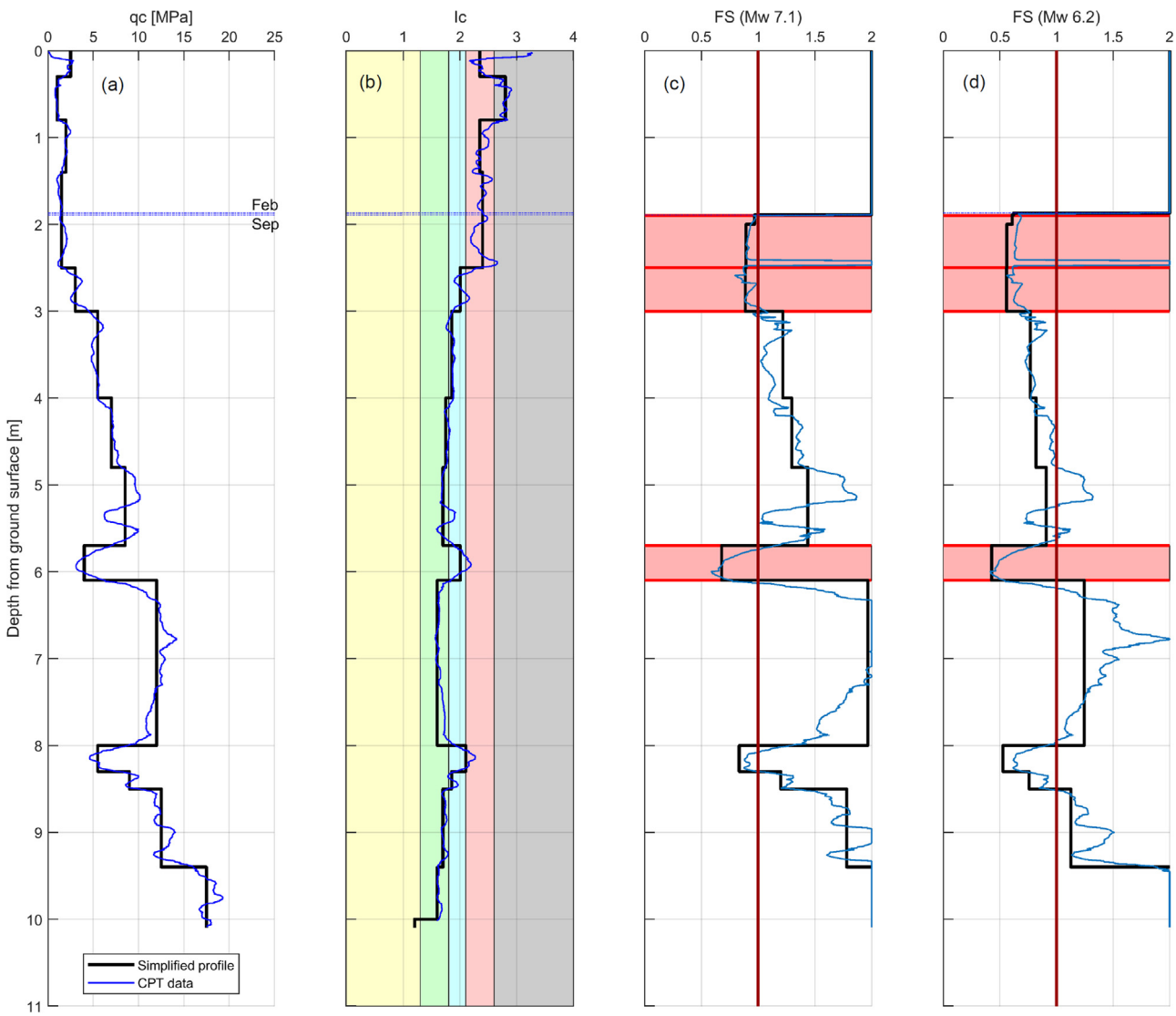

Fig. 3. Determination of critical layer(s) for a simplified profile of an Avondale site: a) q_c values; (b) I_c values; (c) *FS* values for the 4 September 2010 earthquake; (d) *FS* values for the 22 February 2011 earthquake; *potential critical layers shaded in red*. (For interpretation of the references to color in this figure legend, the reader is referred to the web version of this article.).

sites, using Boulanger and Idriss [2] and Robertson and Wride [18] triggering procedures. In the analyses, factors of safety against liquefaction triggering were computed throughout depth, for the top 10 m of the deposits. Typical results of such analyses are shown for the Avondale site in Fig. 3. There are three candidate layers for the *critical layer,* at depths: 1.8–3 m, 5.7–6.1 m, and 8.0–8.3 m. The shallowest layer from 1.8 to 3 m depth appears to be the most likely critical layer from a liquefaction manifestation viewpoint, because it is 1.2 m thick, with low factor of safety, and very close to the ground surface (1.8 m depth). The second candidate layer (5.7–6.1 m depth) has the lowest factor of safety, but is much deeper and thinner, and therefore its manifestation at the ground surface in the absence of liquefaction in the shallow layer is unlikely for the CES events. For the same reason, the deepest layer at 8 m depth was eliminated as a potential critical layer as it is unlikely to manifest liquefaction at the ground surface ahead of the shallower critical layers. Hence, in this case, the shallowest layer was identified as the critical layer, and the second layer at 5.7 m depth was considered as a possible alternative (contributing) critical layer. The above illustrates that the identification of critical layer(s) is not always straightforward, and that in addition to the lowest liquefaction resistance, the position of the layer within the soil profile and its thickness should be considered in the assessment. Clearly, shallow critical layers immediately below or close to the ground surface can most easily manifest liquefaction at the ground surface.

Following the above reasoning, critical layers from a liquefaction manifestation viewpoint were identified for all 55 sites. For several sites, in addition to the shallowest critical layer, one or two additional (alternative) critical layers were also identified, which were at a great depth in the deposit, but showed either similar or slightly lower liquefaction resistance than the principal (shallower) critical layer.

Fig. 4 comparatively shows characteristics of the critical layers for the YY-sites (which manifested liquefaction in both earthquakes) and NN-sites (which did not manifest liquefaction in either event), with box-and-whisker plots. These are weighted-average values for the critical layer for which the thickness of sublayers within the critical layer was used as a weighting factor. It is apparent that, in terms of median values, there is essentially no difference between the critical layers of YY-sites and NN-sites. In fact, the YY-sites and NN-sites have identical median values of their critical layers for the normalized clean-sand equivalent tip resistance (q_{c1Ncs} = 86), soil behaviour type (I_c = 2.15) and depth to the top of the critical layer (z_{CL} = 2.1 m). Hence, the dramatic difference in liquefaction manifestation between the YY-sites

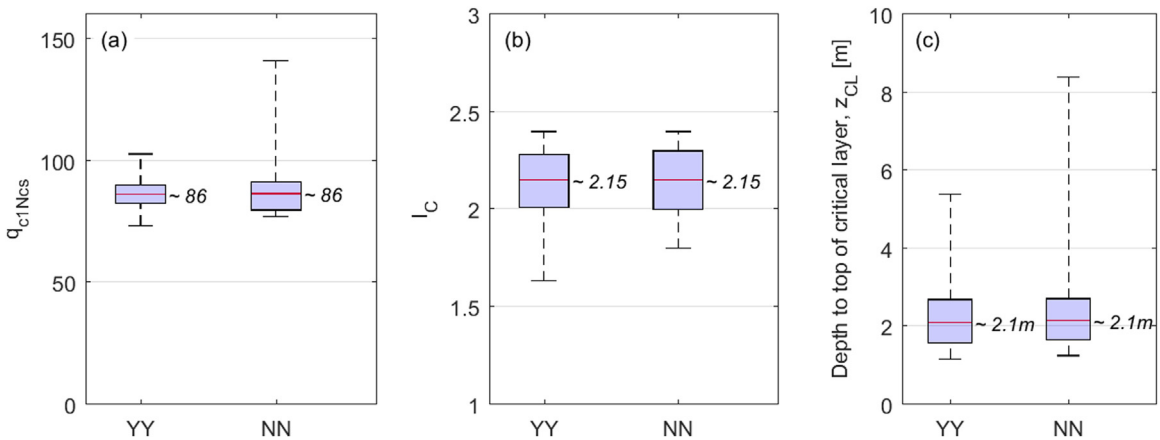

Fig. 4. Comparative illustration of critical layer characteristics for YY-sites and NN-sites using box and whisker plots: (a) clean sand equivalent cone tip resistance (q_{c1Ncs}) of the critical layer; (b) soil behaviour type index (I_c) of the critical layer; (c) depth to top of the critical layer (z_{CL}).

and NN-sites cannot be explained through differences in the characteristics of their critical layers. In both cases, the critical layer is shallow, just two meters below the ground surface, and has low penetration resistance of $q_{c1Ncs} \approx 85$.

2.5. Critical zone and vertical continuity of liquefiable soils

One of the key motivations behind this research was to investigate the effects of system response of liquefiable deposits including interactions between layers at different depths through the dynamic response, pore water pressure dissipation and seepage action due to water flow. In this context, the critical layer represents only one, albeit a significant component in the assessment of liquefiable deposits.

To examine further the characteristics of YY- and NN-deposits in relation to their potential for liquefaction manifestation at the ground surface, a *critical zone* was also defined for each site. The critical zone includes the critical layer but also layers of low liquefaction resistance, which are vertically continuous (connected) and in contact with the critical layer(s). Fig. 5d illustrates the definition of the critical zone for the Avondale site where a continuous zone of relatively low liquefaction resistance is encountered from 1.8 m to 6 m depth, practically connecting the shallow and deep critical layers shown in Fig. 5c. It is anticipated that the critical zone will strongly interact and essentially work as a unit (connected zone) during the development of liquefaction and post-liquefaction through water flow and pore water pressure redistribution. The development of such relatively thick and vertically connected liquefied zone will create conditions for severe liquefaction manifestation through high, continuous and vertically unconstrained excess pore water pressures, with strong upward flow of water towards the ground surface, and consequent soil ejecta.

One may further develop this concept by considering not only a critical zone in the deposit that is anticipated to liquefy during the shaking, but also by considering the thickness and continuity of potentially liquefiable soils throughout the depth of the deposit. This zone of liquefiable materials will encompass the critical zone, but also soils above and below the critical zone that are liquefiable by composition. Such soils are expected to develop excess pore water pressures either due to the cyclic shear stresses induced by the earthquake (e.g. denser sandy soils below the critical zone having $FS > 1.0$) or due to water flow including seepage-induced liquefaction in the shallow soils above the water table. Such zone of liquefiable soils is illustrated in Fig. 5b for the Avondale profile, where nearly all soils in the top ten meters are potentially liquefiable ($I_c < 2.6$). One may anticipate that liquefiable and pore pressure generating soils above and below the critical zone could further exacerbate liquefaction effects and make liquefaction manifestation at the ground surface even more severe.

Fig. 6a, b and c comparatively show the thickness of the critical zone, cumulative thickness of sand layers with $I_c < 1.8$, and cumulative thickness of liquefiable soils ($I_c \leq 2.6$), respectively, for the YY-sites and NN-sites. Unlike the identical characteristics of their critical layers, there are clear differences between the YY-sites and NN-sites with regard to the thicknesses of their critical zones and potentially liquefiable materials. While the median value for the thickness of the critical zone of YY-sites is only slightly larger than the respective thickness of the NN-sites, about 40% of the YY-sites have nearly double thickness of the critical zone. Moreover, majority of the sites that liquefied in both earthquakes (YY-sites) have a vertically continuous zone of liquefiable materials in the top 10 m of the deposit, of which about 6 m (on average) consists of clean sands. The respective thickness of the liquefiable materials for NN-sites is 50% smaller with a median value of approximately 5 m cumulative thickness of liquefiable soils, and cumulative sand thickness of only 1.2 m in the top 10 m of the deposit. Importantly, at the NN-sites the liquefiable layers are vertically discontinuous, interrupted by (sandwiched between) non-liquefiable soils, and capped by a non-liquefiable crust. These features of the YY and NN profiles and their effects on liquefaction manifestation will be rigorously examined using seismic effective stress analyses.

2.6. Summary of general characteristics of YY- and NN-deposits

The YY-sites are generally characterized by vertically continuous liquefiable soils in the top 10 m and shallow water table at about 2 m depth. These deposits are typically composed of a shallow sand layer with some fines in the top 2–3 m, overlying a vertically continuous 7–8 m thick sand or fine sand layer up to 10 m depth. The vertical continuity of liquefiable sands, absence of non-liquefiable layers, including absence of a non-liquefiable crust, are key features of the YY-sites, which manifested liquefaction in both earthquakes. A characteristic soil profile for an YY-site is shown in Fig. 7a.

The NN-sites, on the other hand, are highly stratified deposits consisting of interbedded liquefiable and non-liquefiable soils. A crust of non-liquefiable soil, shallow water table at about 1.0–2.0 m depth, horizontal 'grid' of non-liquefiable layers and vertical discontinuity of liquefiable soils are key features of the NN-sites, which did not manifest liquefaction in either earthquake. Fig. 7b shows a typical soil profile for an NN-site.

3. Representative soil profiles

The analysis and interpretation of the simplified soil profiles of the 55 sites presented above illustrate some general features of the deposits of YY-sites and NN-sites. Importantly, no differences were found with

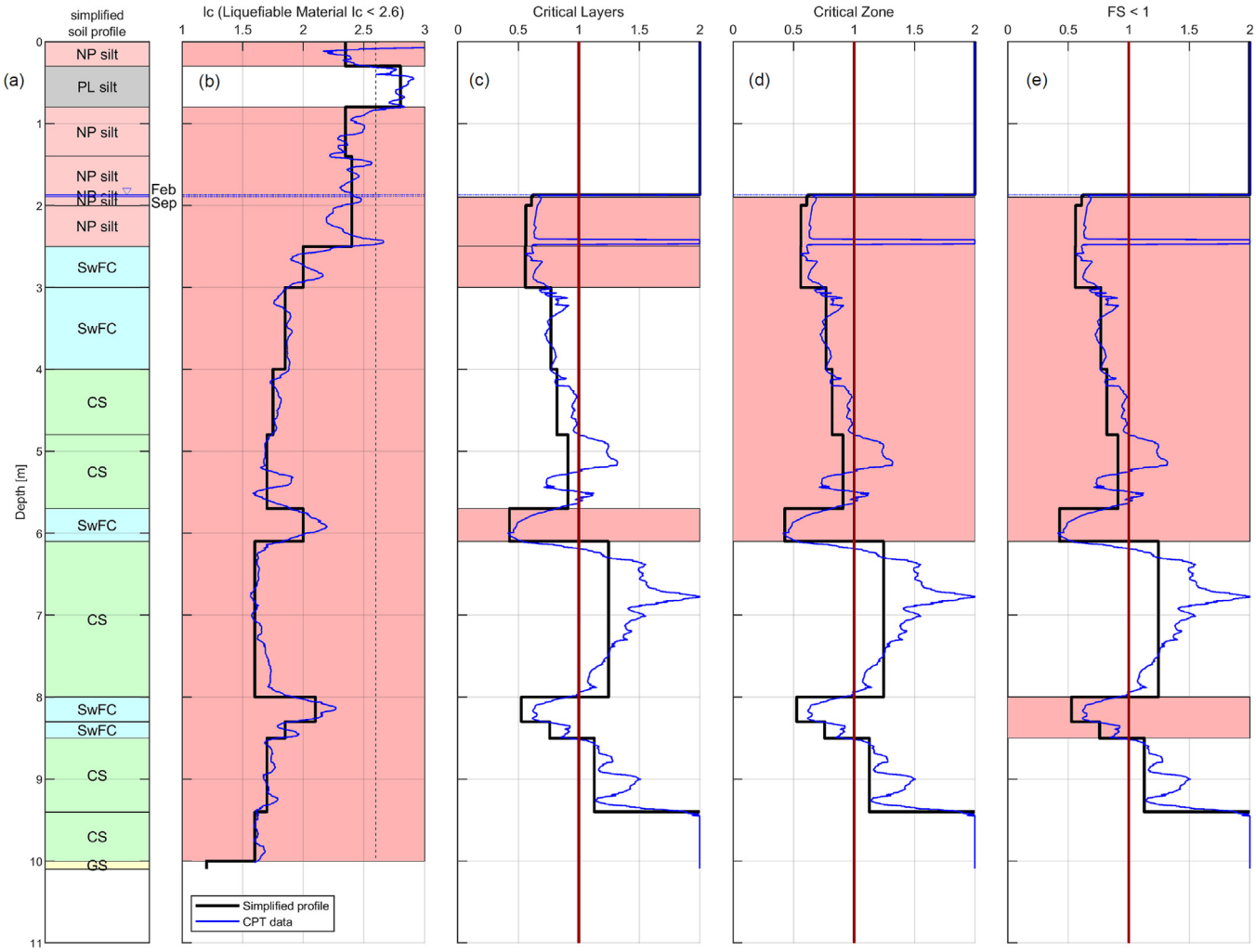

Fig. 5. Determination of critical zone and zone of liquefiable soils (by composition) for a simplified profile: (a) simplified soil profile; (b) I_c profile; (c) critical layers; (d) critical zone; (e) layers with $FS < 1.0$; *critical layers, critical zone and liquefiable soils shaded in red; in plots (c), (d) and (e) FS values for the 22 February 2011 earthquake are shown*. (For interpretation of the references to color in this figure legend, the reader is referred to the web version of this article.).

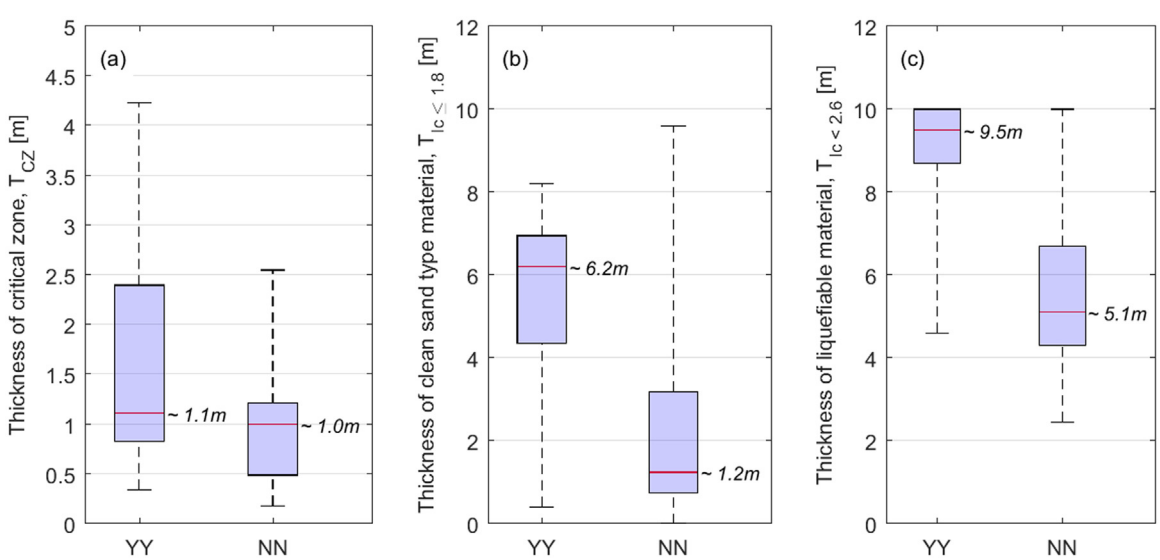

Fig. 6. Comparison of thicknesses of critical zone and liquefiable soils in the top 10 m of YY-sites and NN-sites: (a) thickness of a continuous critical zone, T_{CZ}; (b) cumulative thickness of sand layers with $I_c < 1.8$, $T_{Ic<1.8}$ (c) cumulative thickness of liquefiable materials, $T_{Ic<2.6}$.

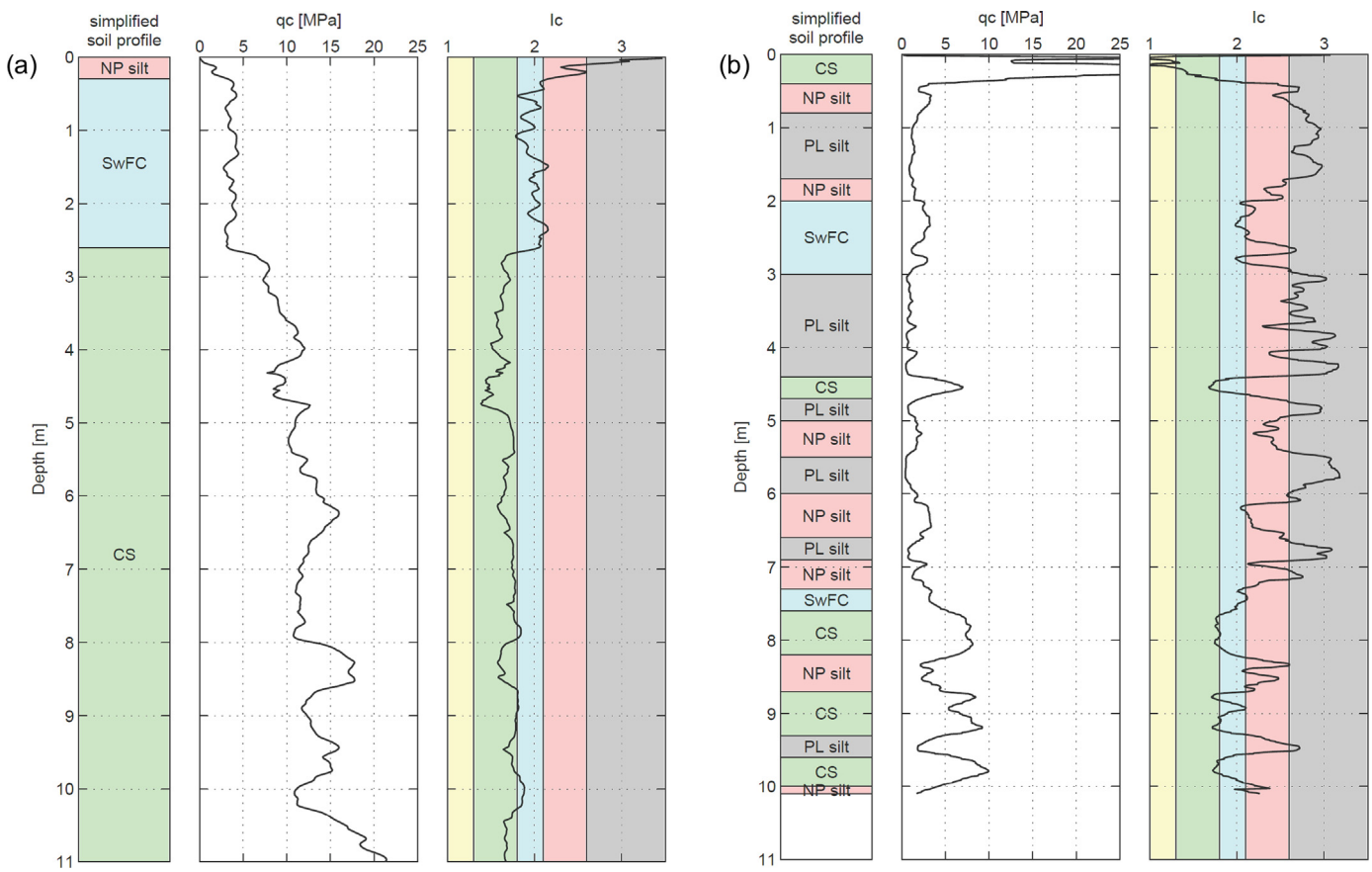

Fig. 7. General characteristics of YY- and NN-deposits: (a) YY-deposits: shallow water table; all layers liquefiable by composition; vertically continuous, thick sand layers; predominantly fine sand; sand with some fines in the top 2–3 m; absence of non-liquefiable crust; manifested liquefaction in both earthquakes; (b) NN-deposits: shallow water table; highly stratified deposits; inter-bedded liquefiable and non-liquefiable soils; sequence of silty sand, silt and non-liquefiable soils; absence of clean sand layers; non-liquefiable crust above ground water table; absence of vertical continuity of liquefiable soils; did not manifest liquefaction in either event.

regard to the depth (z_{CL}) or location of the critical layer within the deposit, and penetration resistance (q_{C1Ncs}) and soil behaviour type index (I_c) of the critical layer. However, the YY-deposits were found to have thicker critical zones and also vertically continuous liquefiable materials in the top 10 m. To further explore the effects of these deposit characteristics rigorous modelling and dynamic analyses were performed using the effective stress analysis method, as described in the following sections.

The simplified soil profiles developed for the 55 sites were organized in three groups based on the liquefaction manifestation during the earthquakes (YY-sites, NY-sites and NN-sites). Each group was then separately scrutinized to identify common characteristics of the deposits, and determine representative soil profiles for the group. In this way, four representative soil profiles were determined: two for the YY-sites, and two for the NN-sites. As discussed earlier, the intermediate NY-sites were not covered in this initial study.

3.1. YY-1 representative soil profile

The 15 sites that manifested liquefaction during both 4 September 2010 and 22 February 2011 earthquakes showed some common characteristics, as summarized in Figs. 4, 6 and 7. Three of the sites, showed presence of non-liquefiable soils and generally had smaller cumulative thickness of the liquefiable materials (4.3–6.3 m, i.e. the whisker for the YY-sites in Fig. 6c). For this reason, these three sites were removed from the considerations, and representative soil profiles for the YY-sites were determined based on the characteristics of the remaining 12 sites. Interestingly, these 12 sites were found to be located in the same general area, in the eastern suburbs of Avonside, Dallington, Avondale and Bexley, along the Avon River. The remaining three sites that showed somewhat different characteristics of the deposits were located in different areas, in Papanui (north-west) and Hoon Hay (south-west).

Further scrutiny of the selected 12 YY-sites identified slight differences in the deposits between two sub-groups, and hence it was decided to define two representative soil profiles for the YY-deposits (YY-1 and YY-2 respectively), as described below.

The normalized clean-sand equivalent cone tip resistance (q_{C1Ncs}) for the four deposits selected to characterize the YY-1 profile is shown in Fig. 8a. The four CPT profiles show some scatter in the q_{c1Ncs} values, but also a relatively well defined and narrow range of tip resistances especially in the zone from 2 m to 6 m depth where the lowest tip resistances were encountered. Based on these data, a simplified profile for the YY-1 sites was defined, as summarized in Fig. 8b, with the following key features:

- The critical layer is located immediately below the water table, from 1.8 m to 3.8 m depth.
- The critical zone is 4.2 m thick (from 1.8 m to 6.0 m depth) and has low tip resistance of $q_{c1Ncs} \approx 80 - 90$.
- There is a gradual increase in q_{c1Ncs} with depth.
- All top 10 m of the deposit are composed of liquefiable soils including the nominal "crust" above the water table and the soils below the critical zone.

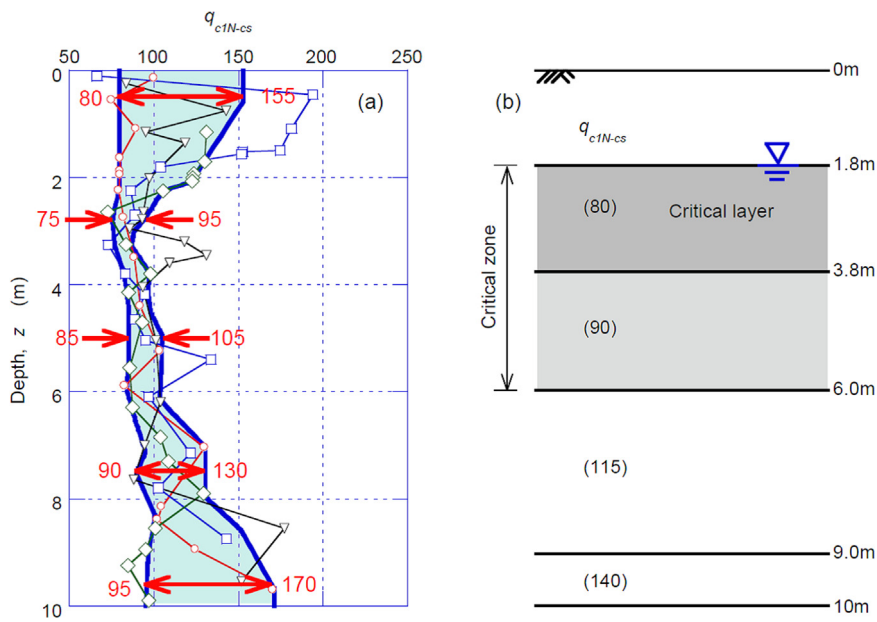

Fig. 8. Characteristics of the representative YY-1 profile: (a) normalized cone tip resistance at four YY-1 sites; (b) representative YY-1 profile (layers and respective q_{c1Ncs} values).

3.2. YY-2 representative soil profile

In a similar fashion, the representative soil profile YY-2 shown in Fig. 9 was determined using six CPT profiles from the remaining eight YY-sites under consideration, based on common characteristics of their deposits. It is apparent from Fig. 9a that larger scatter was observed in the penetration resistance, at a given depth, for the YY-2 profiles, though a clear trend in q_{c1Ncs} with depth is evident. The characteristics of the simplified YY-2 profile shown in Fig. 9b can be summarized as follows:

- The critical layer is located immediately below the water table, from 1.8 m to 2.5 m depth.
- The critical zone is 1.4 m thick (from 1.8 m to 3.2 m depth) and has low tip resistance of $q_{c1Ncs} \approx 85 - 95$.
- There is more pronounced and higher rate of increase in q_{c1Ncs} with depth, as compared to the YY-1 profile.
- All top 10 m of the deposit are composed of liquefiable soils including the nominal "crust" above the water table and the soils below the critical zone.

There are important similarities between the YY-1 and YY-2 profiles, particularly in the shallow location and low penetration resistance of the critical layer, and vertical continuity of liquefiable soils throughout the deposit. On the other hand, the representative YY-2 profile has smaller thicknesses of the critical layer and critical zone than the YY-1 profile, and also slightly higher density of the sandy soils underlying the critical zone.

3.3. NN-1 and NN-2 representative soil profiles

As illustrated by the soil profiles shown in Fig. 7, the NN-profiles are

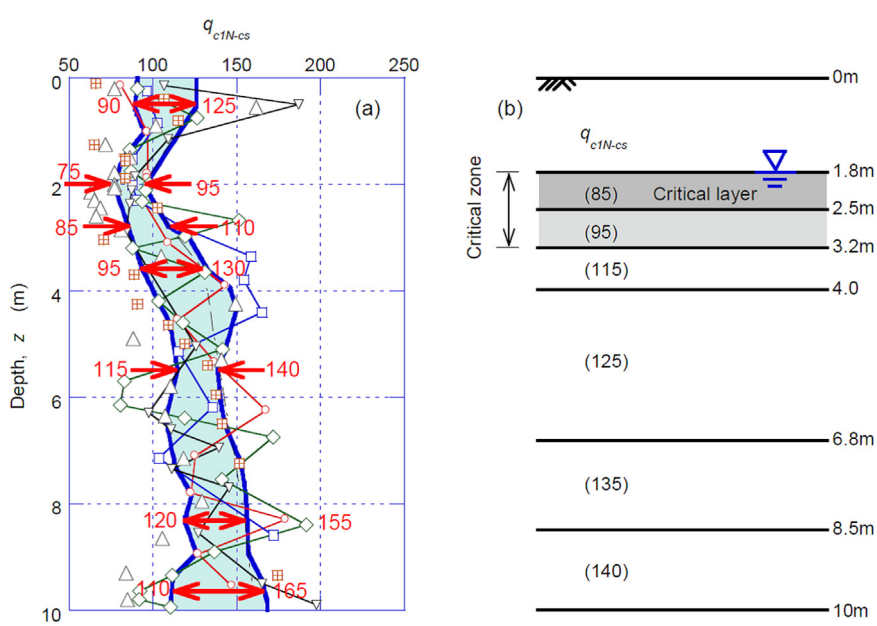

Fig. 9. Representative YY-2 profile: (a) normalized cone tip resistance at six YY-2 sites; (b) stratification and q_{c1Ncs} values of the representative YY-2 profile.

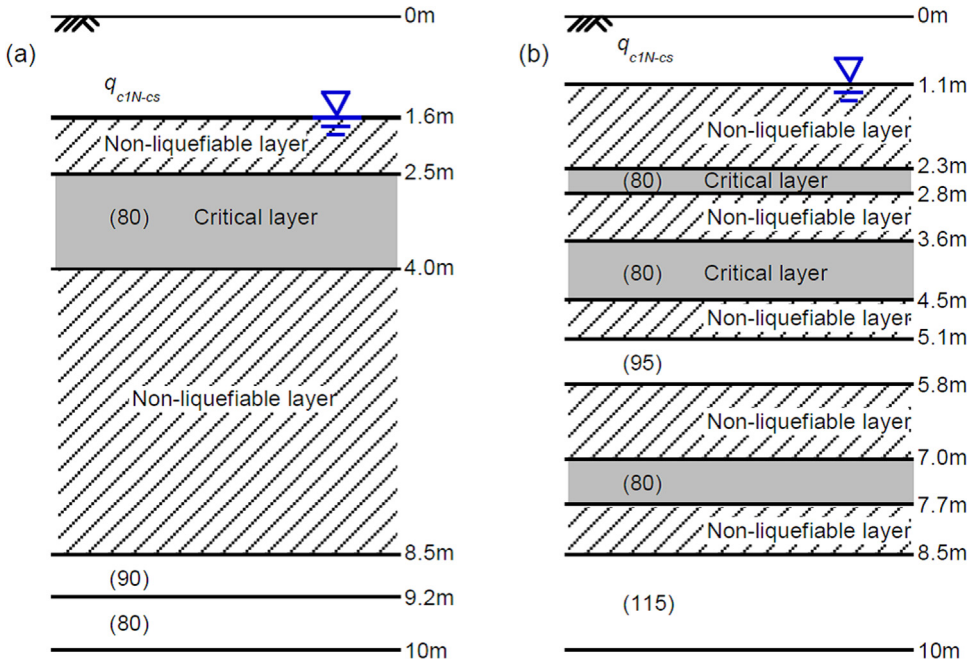

Fig. 10. Layering and q_{c1Ncs} characteristics of the representative NN-profiles: (a) NN-1 profile, characterized by the presence of a relatively thick non-liquefiable layer; (b) NN-2 profile, characterized by a highly stratified deposit with many thin layers of liquefiable and non-liquefiable soils inter-changeably sequenced.

characterized by highly interbedded deposits with relatively fine sequencing of liquefiable and non-liquefiable layers. The liquefiable soils are composed of either fine sand with fines, silty sand or non-plastic silts, whereas clayey soils, plastic silts and peat are typical soils for the non-liquefiable layers. Because of this heterogeneous nature of the NN-deposits, it was difficult to identify two soil profiles that would closely represent the deposits of all 17 NN sites.

The screening process did identify two characteristic types of deposits for the NN-sites, in general terms. One in which a thick non-liquefiable layer was encountered, which was typical for sites in Papanui, Hoon Hay and Halswell, and the other characterized by relatively thin liquefiable and non-liquefiable layers that interchangeably sequenced throughout the depth of the deposit. The thickness of these layers was relatively small, about 0.4–0.8 m for the thinner layers, and 1.0–1.5 m for the thicker layers. This type of highly interbedded deposit was characteristic for the Riccarton area.

Based on the general characteristics of the NN-profiles as above, two particular sites, one in Papanui and the other in Riccarton were selected to determine representative NN-1 and NN-2 profiles, as depicted in Fig. 10. There are several important observations for the representative NN-profiles:

- A shallow critical layer is identified at approximately 2.5–4.0 m depth. The critical layer has low penetration resistance similar to the YY critical layers, with q_{c1Ncs} = 80.
- Low tip resistance (q_{c1Ncs} ≈ 80–90) liquefiable layers also are encountered at greater depths, from 7 m to 10 m depth.
- The liquefiable soils have I_c values predominantly in the range between 2.0 and 2.4, which is consistent with soil behaviour type associated with silty sands and non-plastic silts.
- There is no vertically continuous critical zone or zone of liquefiable soils in the NN-profiles.
- There is a crust of non-liquefiable soil above the critical layer.

4. Effective stress analyses

Using the four representative soil profiles defined in Figs. 8, 9 and 10, numerical models were developed for the YY-sites and NN-sites, and a series of seismic effective stress analyses were performed using 1-D soil-column models to investigate the characteristics of the free-field response at these sites. Principal objectives of these analyses were to capture key features and differences in the responses between the sites that manifested liquefaction in the two earthquakes (YY-sites) and those that did not manifest liquefaction in either event (NN-sites). For a comparison purpose, respective analyses were also performed using the simplified triggering procedure of Boulanger and Idriss [2]. The results of the simplified triggering analyses are only briefly discussed herein, whereas their details can be found in Rhodes [17]. The focus in the following will be on the effective stress analyses and the insights they provide with regard to the performance of the YY-sites and NN-sites.

4.1. Liquefaction resistance of liquefiable soils

As one of the objectives of this study was to develop insights from advanced effective stress analysis that could be used to inform and potentially improve the simplified liquefaction evaluation procedures, a particular approach was adopted allowing for a consistent modelling of liquefaction resistance of soils between the advanced and simplified analyses. In particular, liquefaction resistance curves (LRC), which are used as a key soil property in the calibration of constitutive models for the effective stress analysis, were derived by directly following the simplified liquefaction triggering procedure of Boulanger and Idriss [2], as described below.

The approach adopted in the development of LRC is described for the YY-1 soil profile shown in Fig. 8b. There are five layers in the top 10 m of the YY-1 deposit. The four layers below the water table have q_{c1Ncs} values of 80, 90, 115 and 140 respectively. For each of these layers, an LRC was determined through the following steps:

1) For a given q_{c1Ncs} value, the cyclic stress ratio corresponding to N_c = 15 cycles and effective overburden stress of σ'_{vo} = 100 kPa ($CSR_{Nc=15,\sigma'v=100}$ = $CRR_{M=7.5,\sigma'v=1}$) is estimated using Eq. (1):

Table 2
Estimated b values for the exponent in Eq. (5) based on [2].

q_{c1Ncs}	MSF_{max}	b
80	1.178	0.19
90	1.215	0.21
115	1.351	0.245
140	1.560	0.30

$$CRR_{M=7.5,\sigma'_v=1} = exp\left(\frac{q_{c1Ncs}}{113} + \left(\frac{q_{c1Ncs}}{1000}\right)^2 - \left(\frac{q_{c1Ncs}}{140}\right)^3 + \left(\frac{q_{c1Ncs}}{137}\right)^4 - 2.80\right) \quad (1)$$

2) The maximum value of the magnitude scaling factor (MSF_{max}) is estimated using Eq. (2)

$$MSF_{max} = 1.09 + \left(\frac{q_{c1Ncs}}{180}\right)^3 \leq 2.2 \quad (2)$$

3) The magnitude scaling factor (MSF) is computed over a relevant range of magnitudes using Eq. (3)

$$MSF = 1 + (MSF_{max} - 1)\left(8.64\ exp\left(\frac{-M}{4}\right) - 1.325\right) \quad (3)$$

4) The cyclic stress ratios associated with different MSF values (i.e. magnitudes different than 7.5 or different number of cycles) is estimated using Eq. (4):

$$CSR_{N_c,\sigma'_v=100} = CRR_{M=7.5,\sigma'_v=1} \cdot MSF \quad (4)$$

5) The number of cycles associated with different MSF values (i.e. different magnitudes) is estimated using Eq. (5)

$$N_c = \frac{15}{MSF^{1/b}} \quad (5)$$

In these calculations, the values of the exponent b, summarized in Table 2, were obtained using the $MSF_{max} - b$ relationship proposed in Boulanger and Idriss [2].

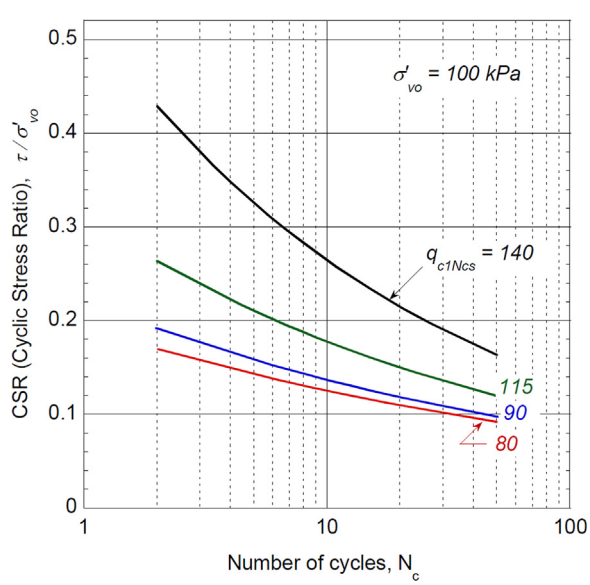

Fig. 11. Liquefaction resistance curves for q_{c1Ncs} values of 80, 90, 115 and 140, and an effective overburden stress of σ'_{vo} = 100 kPa derived based on the simplified triggering procedure of Boulanger and Idriss [2].

Table 3
Estimated K_σ values based on [2].

q_{c1Ncs}	σ'_v (kPa)	C_σ	K_σ
80	40	0.090	1.08
90	60	0.098	1.05
115	80	0.120	1.02
140	102	0.147	1.0

Steps 4 and 5 were used to define $CSR_{Nc,\sigma'v=100}$ - N_c pairs over the range from 2 to 50 cycles; note that the MSF_{max} limit given in Boulanger and Idriss [2] was relaxed to cover CSR values at least from 2 to 30 cycles, as LRC over this range needs to be rigorously simulated in seismic effective stress analyses. In this way, LRCs depicted in Fig. 11 were defined for the representative q_{c1Ncs} values of 80, 90, 115 and 140, for the four layers. Note that these curves are for an effective overburden stress of σ'_{vo} = 100 kPa.

6) In the final step, the LRCs are adjusted for the overburden stress effect by correcting the cyclic stress ratio with the overburden stress correction factor K_σ using Eqs. 6 –8:

$$CSR_{N_c,\sigma'_v} = CSR_{N_c,\sigma'_v=100} \cdot K_\sigma \quad (6)$$

$$K_\sigma = 1 - C_\sigma \ln\left(\frac{\sigma'_v}{P_a}\right) \leq 1.1 \quad (7)$$

where P_a = atmospheric pressure, and

$$C_\sigma = \frac{1}{37.3 - 8.27(q_{c1Ncs})^{0.264}} \leq 0.3 \quad (8)$$

Table 3 summarizes the respective parameters for the four layers of YY-1 profile. The correction for the overburden stress is negligible for the deeper layers, and is relatively small even for the layer with σ'_v = 40 kPa.

4.2. Constitutive model parameters and calibration

An elastic-plastic constitutive model (Stress-Density Model) tailored for liquefaction problems was employed in the effective stress analyses [4,5]. The Stress-Density Model (S-D Model) is a state-concept based model that accounts for the combined effects of density and confining stress on sand behaviour through the state-concept framework. The benefit of this, in addition to the consistent modelling of stress-density effects on sand behaviour, is that the model is a true material model with a single set of parameters representing a given soil across all relevant density-stress states. Soil properties required for the S-D Model fall into four categories: critical state line (used to define the state of the soil relative to the reference state, the critical state); plastic stress - strain parameters (defining the shear stress – plastic shear strain relationship); stress – dilatancy parameters (providing the link between plastic shear strain and plastic volumetric strain increments); and, elastic parameters (determining an incremental stress-strain relationship for elastic behaviour).

The S-D Model parameters are usually determined either through a series of laboratory tests on the target soils, or through a combined use of empirical relationships and generic data for sandy soils. The second approach was adopted in this initial modelling attempt. Christchurch soils were modelled using model parameters established from laboratory tests on Toyoura sand [4,5] as a basis. Two dilatancy parameters of S-D Model were then slightly modified to simulate the target liquefaction resistance curves (LRCs) for the four soil layers determined based on the simplified liquefaction triggering procedure of Boulanger and Idriss [2], as described in the previous section. Fig. 12 comparatively

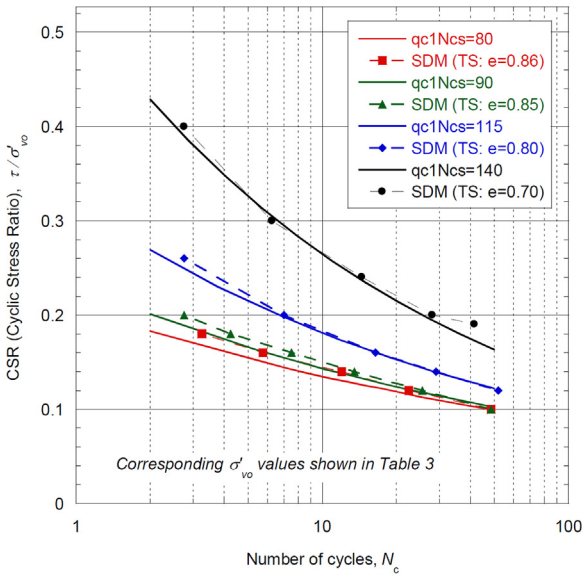

Fig. 12. Target LRCs (solid lines) and model simulations (dashed lines with symbols) for the four characteristic soil layers of YY-1 deposit.

shows the target LRCs (solid lines) and simulated curves with S-D Model (dashed lines with symbols) for the four layers with q_{c1Ncs} values of 80, 90, 115 and 140. In the simulations, different void ratios of $e = 0.86$, 0.85, 0.80 and 0.70 respectively were adopted, in conjunction with the effective overburden stresses corresponding to the depth of each layer (Table 3). A reasonable agreement between the simulated and target curves can be seen in Fig. 12, which is sufficiently accurate for the purpose of this study.

In this way, the elastic-plastic model was calibrated to produce liquefaction resistance curves that are fully compatible with the definition of liquefaction resistance in the simplified triggering procedure of Boulanger and Idriss [2]. The procedure described above provides means for calibrating elastic-plastic constitutive models based on Boulanger and Idriss [2], and hence provides basis for a rigorous comparison of outcomes of effective stress analyses and simplified triggering procedures.

4.3. Modelling of non-liquefiable and deeper layers

Non-liquefiable layers were also modelled with the S-D Model except that the pore pressure generation feature was turned off for these layers. The initial shear modulus was defined based on the measured shear wave velocity in the high-resolution cross-hole testing. The shear stress - shear strain relationships were defined based on model simulations of generic stiffness degradation curves defined by Darandeli [11], modified for strength compatibility at large strains [24]. A PI value of 9 was adopted to define the target stiffness degradation and damping curves for the simulation of stress-strain characteristics of all non-liquefiable layers. In this way, model parameters were defined for all non-liquefiable layers in the top 10 m of the NN-1 and NN-2 profiles.

The 1-D soil-column models used in the effective stress analyses represented the top 20 m of the deposit, and input motions were applied at the base of the model, at 20 m depth. Using several deeper CPTs, characteristic layers from 10 m to 20 m depth were identified, and these layers were modelled following the procedure described above for non-liquefiable soils. Hence, all four representative soil profiles (YY-1, YY-2, NN-1 and NN-2) had identical soil profiles and model parameters from 10 m to 20 m depth. The intention of the adopted approach was to focus on the top 10 m of the deposits, because liquefaction manifestation is governed by the shallow parts of the deposit. This is a well-document general observation, as for example, in the updated database of liquefaction manifestation case histories of Boulanger and Idriss [2], out of over 250 CPT-based case histories there is only one case in which the depth of the critical layer (liquefaction) was greater than 10 m.

Table 4
Adopted permeability (k) values.

Soil behaviour type	I_c	*k (m/s)*
Fine sand - sand with silt	1.8 – 2.2	1×10^{-4}–3×10^{-4}
Sandy silt / silt	2.2 – 2.6	4×10^{-6}
Non-liquefiable soil[a]	> 2.6	1×10^{-7}

[a] Plastic silt or clayey soil.

4.4. Drainage conditions and permeability values

In the effective stress analyses, the soil was treated as a two-phase medium based on Biot's equations for dynamic behaviour of saturated porous media [1]. The analyses were performed under drained conditions allowing for pore water pressure redistribution and vertical water flow through and between layers. Table 4 summarizes the permeability values adopted in the soil column models for characteristic soil behaviour types. Note that for the short durations considered in these analyses, i.e. about 50 s during the shaking and immediately after the shaking, the behaviour of the non-liquefiable layers was effectively undrained, because of the low permeability adopted for these layers.

4.5. Input motions and analysis cases

A ground motion recorded at the Canterbury Aero Club (CACS) strong motion station during the 22 February earthquake, was deconvoluted to the underlying stiffer Riccarton Gravel layer, and was then scaled to approximately 0.20*g*, 0.30*g* and 0.40*g* [17]. These three input motions were used as base excitations of the soil-column models, for each of the four representative soil profiles (YY-1, YY-2, NN-1 and NN-2), resulting in a total of twelve effective stress analyses. Simple shear conditions were enforced in the analyses by tying the nodes of the soil-column model at identical elevations to share identical displacements, and hence simulate free field level ground conditions.

5. Analyses results for YY-profiles

Selected results from some of the twelve effective stress analyses are presented in the following to illustrate key features of the responses of the YY- and NN-profiles with regard to liquefaction development and liquefaction manifestation in particular.

5.1. YY-1 analyses at 0.4g

Fig. 13 shows acceleration and excess pore water pressure (EPWP) time histories computed throughout the depth of the YY-1 profile, for the analysis with the highest intensity input motion of 0.4*g*. The excitation has relatively high accelerations from approximately 6–14 s, and liquefaction rapidly develops in the critical zone over only a few cycles of strong shaking, from 6 to 10 s. Excess pore water pressures at specific time sections, and maximum shear strains are shown in Fig. 14, for the top 10 m of the deposit. Excess pore water pressures develop rapidly throughout the depth of the deposit, and at $t = 10$ s the critical zone of the deposit from 1.8 m to 6.0 m depth liquefies. Following the liquefaction, the excess pore pressures within this zone remain at the level of the initial effective overburden stress (σ'_{vo}), from approximately 35 kPa at the top of the critical zone, to about 65 kPa at 6.0 m depth. The liquefaction results in large maximum shear strains of about 3–4% in the critical zone (Fig. 14b).

The increase in the penetration resistance from q_{c1Ncs} = 80–90 (within the critical zone) to 115 and 140 (below the critical zone) with

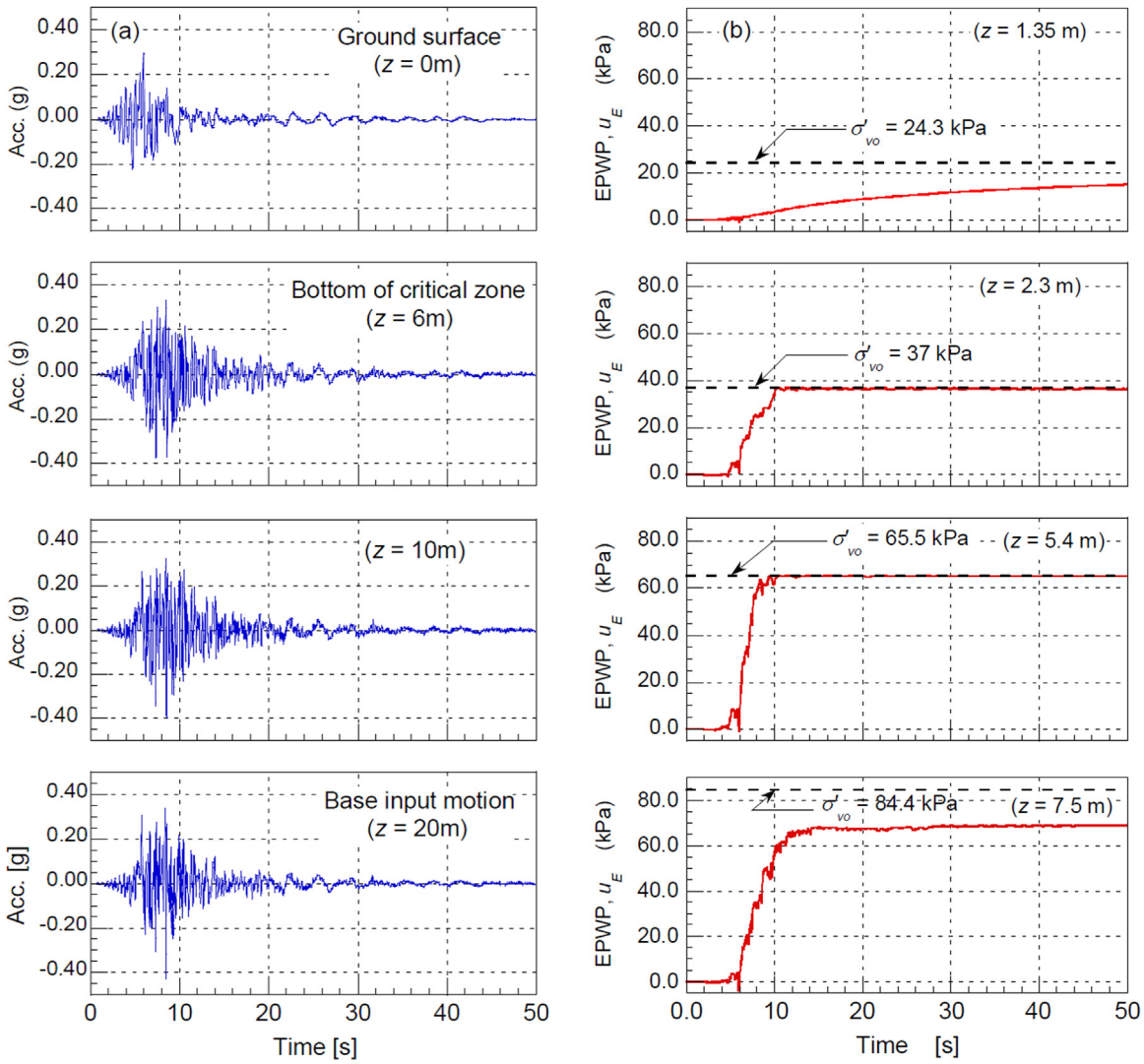

Fig. 13. Acceleration and excess pore water pressure time histories computed throughout the depth of YY-1 profile in the analysis with 0.4*g* base input motion: (a) accelerations; (b) excess pore water pressures.

depth in the YY-1 profile, and consequent increase in the liquefaction resistance shown in Fig. 12, prevented liquefaction from developing at depths greater than 6 m depth. Fig. 14b shows that the maximum shear strains at depths greater than 6 m were less than 1%. However, it is important to note that despite not causing liquefaction at these greater depths, the excess pore pressures at depths from 6 m to 10 m reached about 70 kPa and were (substantially) higher than the 35–65 kPa excess pore water pressures in the overlying critical zone. This implies an upward gradient and significant water flow from the underlying deeper layers from 6 m to 10 m depth into the critical zone, which will cause additional disturbance including prolonged and more severe fluidization of the already liquefied soils in the critical zone. In addition, gradual increase in the excess pore water pressures is seen in the top part of the deposit (above the initial water table depth of 1.8 m) in Figs. 13b and 14a due to an upward flow of water from the liquefied critical layer towards the ground surface.

Fig. 15 schematically illustrates principle mechanisms that lead to severe liquefaction manifestation at the ground surface of the YY-1 profile. It involves the following key processes and consequences:

(1) First, liquefaction rapidly develops in the critical zone from 1.8 m to 6.0 m depth during a few seconds of strong shaking. The liquefaction results in zero effective stress, loss of particle contact and skeleton structure or *true liquefaction* associated with loose sandy soils (q_{c1Ncs} = 80) in the critical zone.
(2) The already liquefied soil in the critical zone is then subjected to substantial additional disturbance due to seepage action and upward flow of water from the underlying layers into the critical zone. This water inflow under high pressures exacerbates the fluidization and instability of the soil structure in the liquefied critical zone.
(3) Finally, the soil above the water table at shallow depths below the ground surface (from 0 m to 1.8 m depth), liquefies and loses its effective stress due to an upward water flow from the critical zone towards the ground surface (seepage-induced liquefaction). This effectively creates a liquefied zone from the ground surface to 6 m depth that receives an additional influx of water from the deeper part of the deposit, from 6 m to 10 m depth.

These mechanisms involving vertical communication of excess pore water pressures and large volumes of water can explain the severe liquefaction effects that were observed at the YY-sites. They are characterized by a pronounced interaction between layers and system response in which the whole deposit contributes to the severity of liquefaction manifestation at the ground surface.

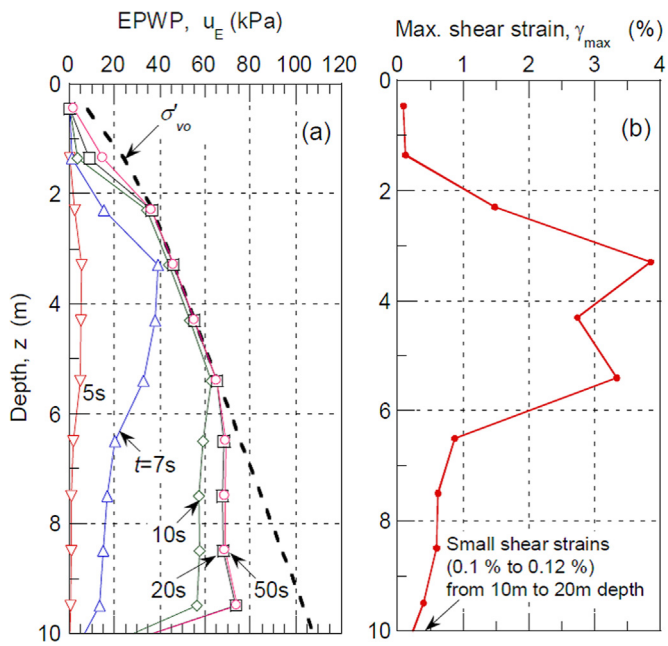

Fig. 14. Response characteristics of YY-1 profile subjected to 0.4*g* base input motion: (a) evolution of excess pore water pressures throughout the depth of the profile with time; (b) maximum shear strains throughout the depth of the deposit.

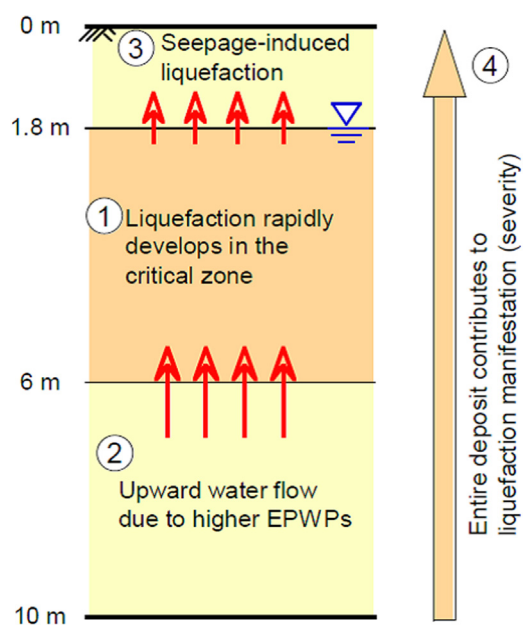

Fig. 15. Schematic illustration of system-response mechanisms intensifying liquefaction manifestation for YY-1 profile.

5.2. YY-1 analyses at lower excitation levels

Fig. 16a and b show the excess pore water pressures at $t = 20$ s and maximum shear strains, respectively, computed in the analyses of the YY1-profile with 0.2*g*, 0.3*g* and 0.4*g* maximum base accelerations. The results for the smaller excitation levels of 0.2*g* and 0.3*g* are generally consistent with the lower demands imposed in these analyses.

The results of the analysis with 0.3*g* input acceleration were essentially identical with regard to the mechanisms described above and depicted in Fig. 15. For the smallest excitation level of 0.2*g*, only part of the critical layer (from 2.8 m to 3.8 m depth) liquefies during the strong shaking in the first 20 s. It is apparent from Fig. 16a that the excess pore

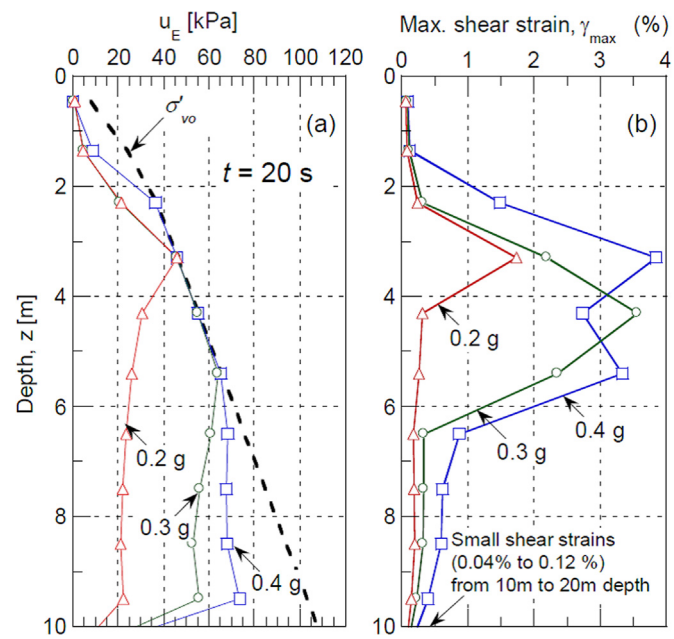

Fig. 16. Response characteristics throughout the depth of YY-1 profile in analyses with base input motions of 0.2*g*, 0.3*g* and 0.4*g*: (a) excess pore water pressures at $t = 20$ s; (b) maximum shear strains.

water pressures are the highest in the liquefied layer, and hence, the water from this layer will flow upwards and downwards at this stage. In other words, the second mechanism depicted in Fig. 15 will not eventuate in this case. This feature in conjunction with the much smaller thickness of soils that liquefied, smaller shear strains in the liquefied soil, and much lower excess pore water pressures throughout the depth of the deposit is expected to result in lower severity of liquefaction manifestation on the ground surface as compared to the previously presented reference case for 0.4*g*. Hence, accelerations (seismic demand) above certain thresholds are needed to trigger specific system response mechanisms and consequent increase in the severity of liquefaction manifestation.

5.3. YY-2 analyses

Consistent results, essentially identical trends, and response characteristics were observed in the YY-2 analyses with those presented for the YY-1 profile. The only notable difference in the response was the smaller thickness of the liquefied zone due to the thinner critical zone (1.8–3.2 m depth) and higher density of the layers underlying the critical zone, as depicted in Fig. 9 for the YY-2 profile.

6. Analyses results for NN-profiles

6.1. NN-1 analyses

A shallow critical layer from 2.5 m to 4 m depth, thick non-liquefiable layer from 4 m to 8.5 m depth, and deep layers with similarly low q_{c1Ncs} values as those of the critical layer from 8.5 m to 10 m depth, characterize the NN-1 profile (Fig. 10a). The shallow layer with low penetration resistance is critical with regard to liquefaction manifestation, however both the shallow and deep loose layers are relevant for liquefaction triggering and its consequent effects on the dynamic response of the deposit. The analyses results depicted in Fig. 17 show that both loose layers rapidly develop excess pore water pressures and liquefy after only few cycles of strong shaking (from $t = 6$–10 s). The maximum shear strains are consistent with the development of liquefaction in these layers and are slightly larger in the deeper layers.

Fig. 17c illustrates important effects of dynamic interaction

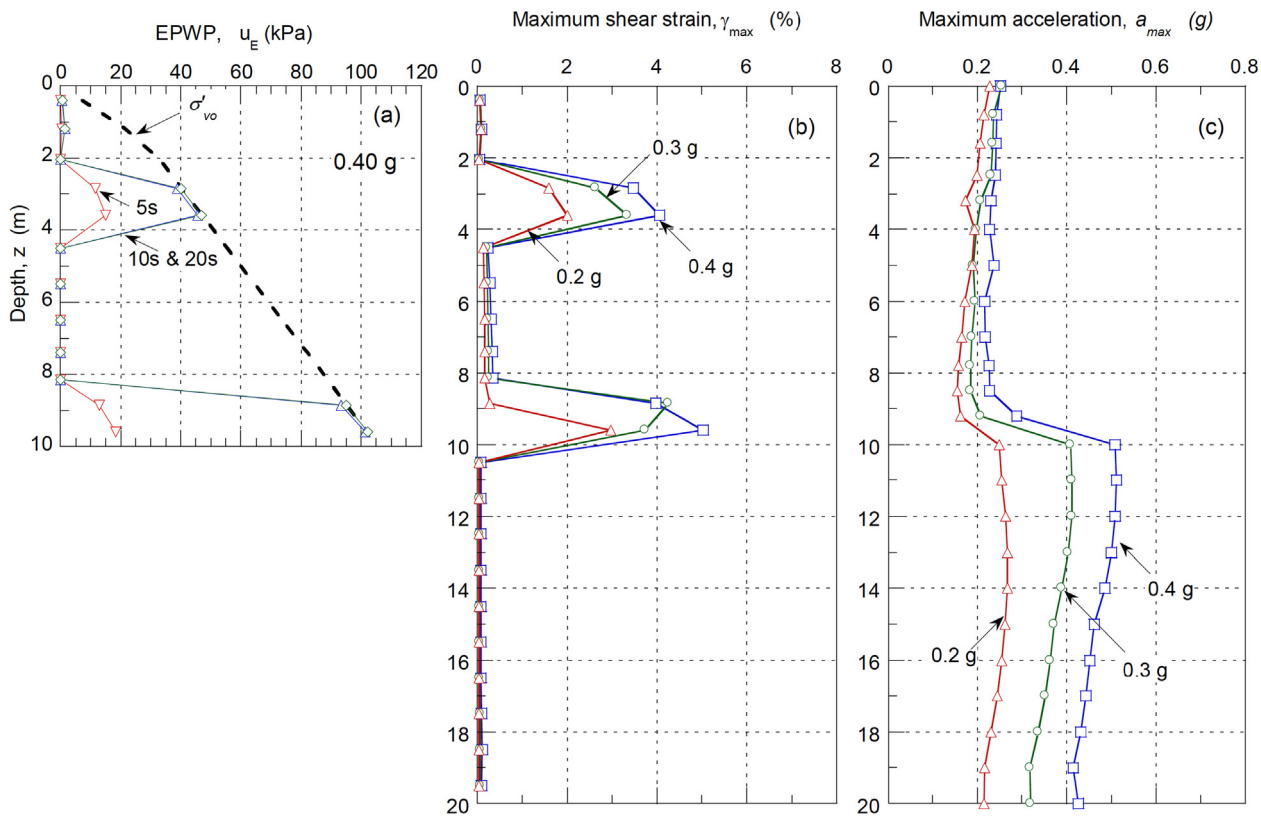

Fig. 17. Response characteristics throughout the depth of NN-1 deposit in analyses with base input motions of 0.2*g*, 0.3*g* and 0.4*g*: (a) evolution of excess pore water pressures (for 0.4*g* only); (b) maximum shear strains; (c) maximum accelerations.

throughout the deposit, where a substantial reduction in accelerations from 10 m to 8.5 m depth is seen due to the softening and liquefaction of the deep loose layer. This in turn results in a large reduction of the demand for all soils above these layers (i.e. above 8 m depth). Note that such cross-interaction effects in the dynamic response are not accounted for in the simplified method of liquefaction evaluation.

6.2. Effects of partial saturation

The V_p measurements from the high-resolution cross-hole testing provided important observations with regard to the degree of saturation of the YY- and NN-deposits. The data are not presented herein, but key observations can be summarized as follows: (a) non-liquefiable soils showed compressional velocities consistent with partial saturation (substantially lower than 1500 m/s) from the groundwater table up to 6–7 m below it; (b) silty soils showed larger propensity for partial saturation, with a substantial portion of such soils showing partial saturation at depths within 3–5 m from the water table; (c) sands predominantly showed full saturation, except for a very shallow portion of about 0.5–1 m immediately below the water table. Hence, NN-deposits could be partially saturated over a substantial depth below the water table.

Partial saturation is known to increase the liquefaction resistance due to an increased compressibility of the soil-skeleton and consequent reduction in pore pressure generation during cyclic loading (e.g. [20]). To investigate the potential effects of partial saturation on the response of NN-1 deposits, a sensitivity study was performed in which the shallow critical layer was the subject of the sensitivity analyses. Note that the shallow critical layer is sandwiched between two non-liquefiable layers, and hence is likely to be affected by the partial saturation in the shallow part of the deposit.

In the series of analyses, the liquefaction resistance of the critical layer was incrementally increased in each analysis so that it was providing 10%, 20%, 30%, etc. higher resistance than the reference LRC for a fully saturated critical layer. The objective of these incremental analyses was to identify a percentage increase in CRR required to prevent occurrence of liquefaction in the shallow critical layer. Fig. 18 shows EPWP time histories throughout the depth of the NN-1 deposit for an analysis in which the LRC of the critical layer was increased for 35% relative to the fully saturated LRC reference. The results show that, in this case, the critical layer did not liquefy, and that the maximum EPWPs in this layer reached about 65–77% of the initial effective overburden stress.

Fig. 19 summarizes the results of the sensitivity analyses. It shows the EPWP ratio (u_E / σ'_{vo}) and respective maximum shear strain (γ_{max}) computed in the incremental analyses. The results indicate that liquefaction would not occur in the critical layer if its *CRR* was about 25–30% higher than the reference *CRR* value for fully saturated soil shown in Fig. 12. Detailed studies are currently under way using high-resolution V_p data from the 55 sites and lab testing of partially saturated Christchurch soils to better quantify the effects of partial saturation on *CRR*.

6.3. System response of NN-deposits

Fig. 20 schematically illustrates the response mechanisms leading to no liquefaction manifestation at the ground surface of NN-sites. It involves the following key processes and effects:

(1) Liquefaction triggering first occurs in a deeper layer (below 8 m depth) of fully saturated liquefiable soils of low penetration resistance (q_{c1Ncs} = 80–90).
(2) The liquefaction of the deep layer results in a substantial reduction of accelerations and seismic demand for all layers in the top 8 m of the deposit.
(3) Partial saturation of the inter-bedded deposits containing non-

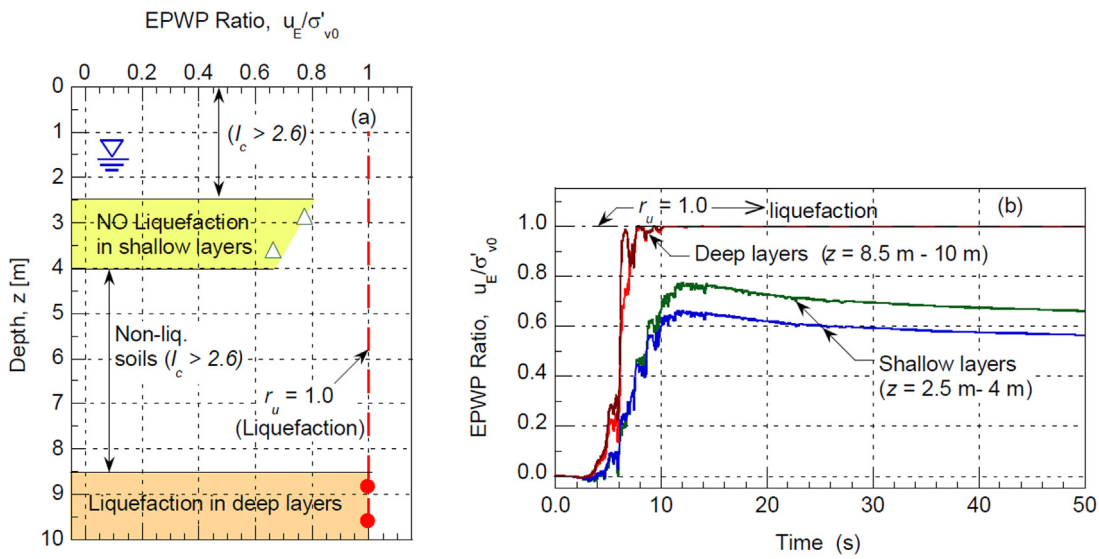

Fig. 18. Computed excess pore water pressure ratios throughout the depth of the NN-1 model in analysis with base input motion of 0.4 g and increased liquefaction resistance in the shallow liquefiable layer to 1.35 × *CRR* of a fully saturated soil: (a) distribution throughout depth of deposit; (b) time histories.

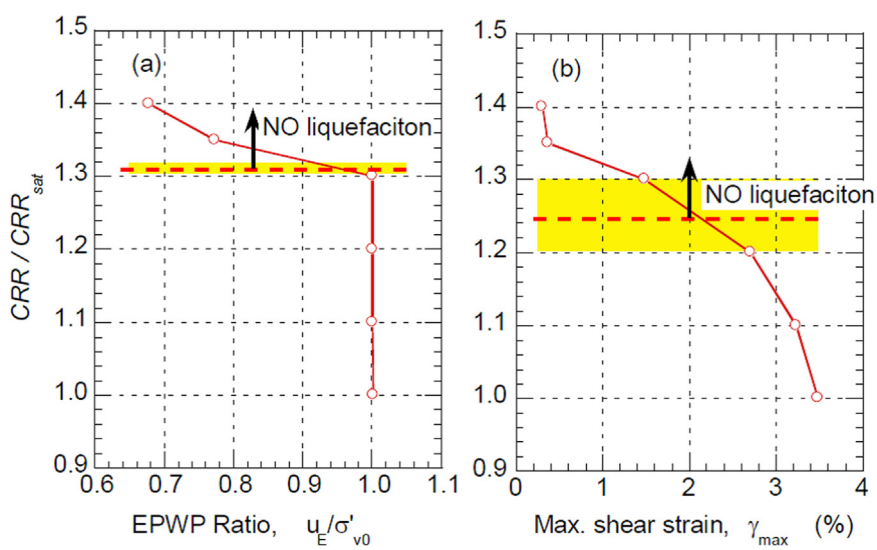

Fig. 19. Results from sensitivity analyses on the effects of an increase in CRR in the shallow critical layer on: (a) maximum excess pore water pressure ratios (b) maximum shear strains in the layer.

liquefiable and some liquefiable soils may sufficiently increase the liquefaction resistance of the shallow critical layer to prevent occurrence of liquefaction in this layer in conjunction with the reduction in the seismic demand, as above. This effectively results in a non-liquefied crust from the ground surface to 8.5 m depth, and therefore, the liquefaction at depth below 8.5 m would be unlikely to manifest at the ground surface for the seismic demand imposed by the M_w*6.2* February earthquake.

Importantly, for the NN-deposits, there is absence of vertical continuity and 'communication' of critical layers and liquefiable soils, or development of system-response mechanisms that intensify the severity of liquefaction manifestation at the ground surface. Conversely, the above three system-response features of the NN-sites mitigate the development of liquefaction and its manifestation at the ground surface. The lack of vertical continuity and communication of excess pore water pressures of liquefiable soils was also a key feature observed in the NN-2 analyses [10].

7. Results from simplified analyses

Simplified liquefaction analyses were performed for the 55 sites in which factors of safety against liquefaction triggering and liquefaction damage indices, *LPI* and *LSN*, were estimated for the 4SEP2010 and 22FEB2011 earthquakes. Fig. 21 summarizes the computed *LPI* and *LSN* values in terms of box-and whisker plots, separately for the 4SEP2010 and 22FEB2011 earthquakes, for YY-sites and NN-sites. It is evident from this figure that out of the 34 cases for the NN-sites (17 sites for two events), both *LSN* and *LPI* correctly predicted no occurrence or minor liquefaction for only 3 cases (9% of the cases), whereas for 31 cases (91% of the cases) liquefaction manifestation was heavily over-estimated. For most of the no-liquefaction manifestation sites (NN-cases) major to severe liquefaction was predicted. Conversely, for the YY-sites, the simplified analyses under-estimated the observed liquefaction manifestation in 50% of the cases (11 out of 22 predictions). The opposite biases towards systematic under-prediction for YY-sites and over-prediction for NN-sites are consistent with the lack of consideration of system-response effects in the simplified liquefaction evaluation procedures involving mechanisms that intensify liquefaction

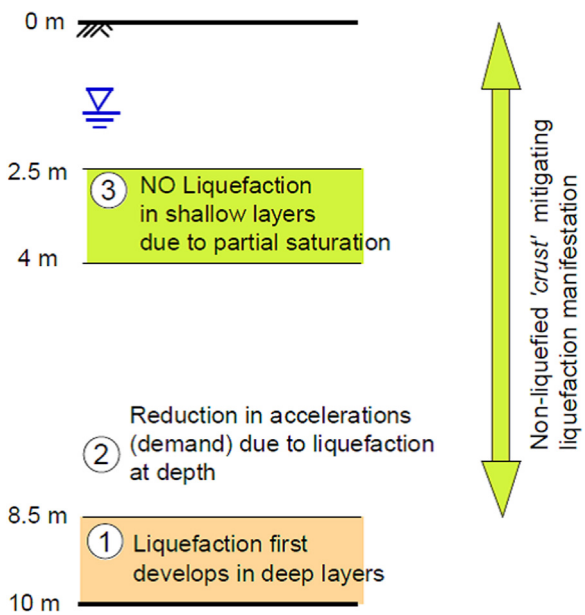

Fig. 20. Schematic illustration of key mechanisms mitigating liquefaction manifestation for NN-1 profile.

manifestation for YY-sites and mechanisms that mitigate liquefaction manifestation for NN-sites. The significant number of mispredictions emphasizes the importance of system-response effects on liquefaction manifestation and the need for their incorporation into liquefaction assessment. The summary of the predictions based on simplified analyses using *LSN* is given in Table 5.

8. Conclusions

The following key findings can be summarized from the presented study on the 55 Christchurch sites.

(1) There are no differences in the characteristics of the critical layers between the sites that manifested liquefaction in both earthquakes (YY-sites) and the sites that did not manifest liquefaction in either event (NN-sites). For both YY and NN sites, the critical layer has low tip resistance ($q_{c1Ncs} \approx 80$–86) and is located at shallow depth of approximately 2.0 m below the ground surface.

(2) The YY-sites and NN-sites have important differences with regard to their deposit characteristics. YY-sites have relatively thick critical zones of low liquefaction resistance in deposits entirely composed of liquefiable soils in the top 10 m. This ensures vertical continuity of liquefiable soils with low liquefaction resistance and soils with high potential to generate significant excess pore water pressures. Conversely, the NN-sites are interbedded deposits of liquefiable and non-liquefiable soils. Because of this vertical discontinuity, NN-sites effectively have no critical zones or liquefiable zones combining two or more layers.

(3) Results from effective stress analyses identified a characteristic system response of YY-sites involving: (i) rapid liquefaction of the shallow critical layer; (ii) additional disturbance of the liquefied critical layer due to seepage action and inflow of water from the underlying layers that didn't liquefy, but generated higher excess pore water pressures than those in the critical layer; and, (iii) vertically unconstrained water flow, and seepage-induced liquefaction in shallow soils above the water table. These mechanisms and processes effectively result in a strong and damaging discharge of excess pore water pressures in which liquefiable soils from the entire deposit contribute to and intensify the severity of liquefaction manifestation at the ground surface.

(4) A threshold seismic demand level is required to generate higher excess pore pressures in the soils underlying the critical zone. For seismic demand above this threshold level, one may anticipate a step increase in the severity of liquefaction due to inflow of water

Table 5
Summary of results from simplified analyses (*LSN predictions*).

LSN-based Prediction[a]	YY-sites (11)	NN-sites (17)
Good agreement	50%	9%
Under-estimation	50%	–
Over-estimation	–	91%

[a] Agreement between predictions and observations.

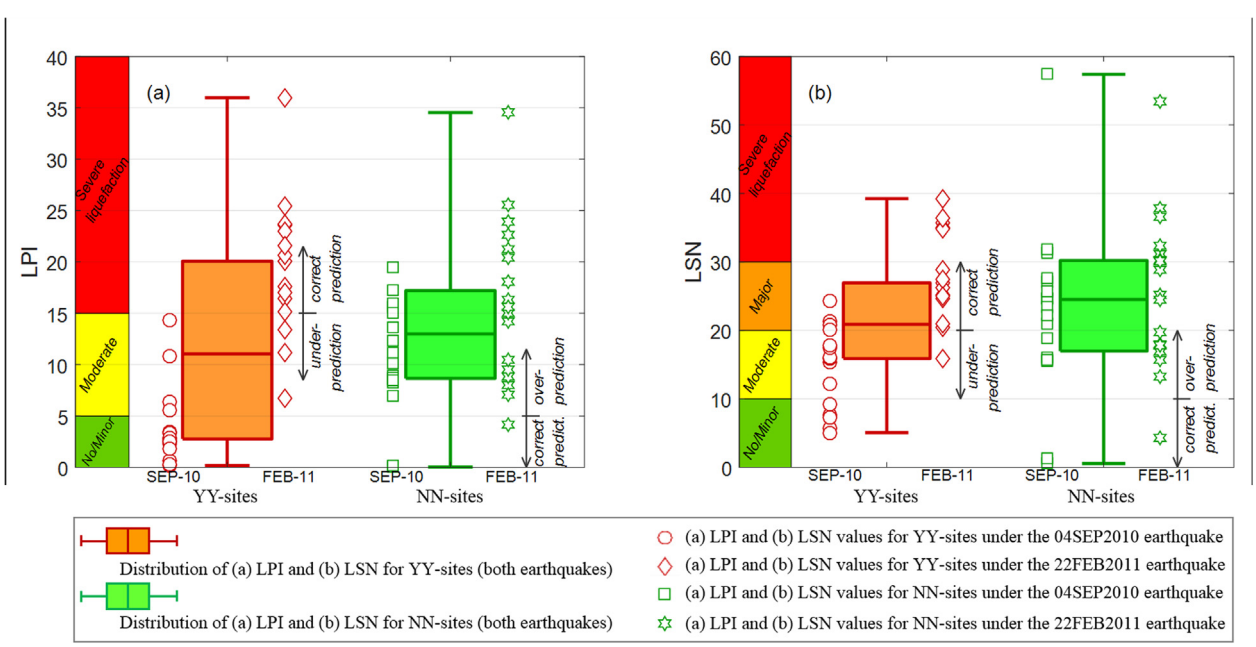

Fig. 21. Box and whisker plots summarizing results from simplified analyses in terms of estimated liquefaction-damage indices for YY-sites and NN-sites, for the 4 September 2010 and 22 February 2011 earthquakes: (a) *LPI* values; (b) *LSN* values.

into the liquefied critical layer and prolonged disturbance (fluidization) of the liquefied soil (and consequent activation of the second mechanism depicted in Fig. 15).

(5) Effective stress analyses of the NN-sites identified a system response of the deposit involving: (i) dynamic cross-interaction between layers, where liquefaction in a deeper layer (8–10 m depth) substantially reduces the demand for all soils above that depth; (ii) isolation or vertical confinement of layers that liquefy or develop high excess pore pressures, by capping and underlying non-liquefiable layers; (iii) partial saturation of non-liquefiable soils, liquefiable silty soils and NN-deposits as a whole in the top 3–5 m, which in turn increases the liquefaction resistance of shallow critical layers. Here, not only an increase in CRR, but also effects of partial saturation through stiffening of shallow soils and consequent reduction in shear strains should be considered.

(6) System responses of YY and NN deposits are characterized by cascading mechanisms and effects. However, the cascading effects work in opposite directions for the YY and NN sites with regard to liquefaction manifestation. For YY-sites, the system response increases the severity and consequences of liquefaction through the processes described in Item 3. Conversely, for the NN-sites, the mechanisms summarized in Item 5 contribute to reduction in the likelihood for development of liquefaction and its manifestation at the ground surface.

(7) Current simplified liquefaction evaluation procedures systematically over-estimated liquefaction manifestation for NN-sites, and underestimated liquefaction manifestation for YY-sites. These tendencies in the mispredictions reflect the fact that simplified procedures ignore system response effects that mitigate liquefaction manifestation for NN-sites and intensify liquefaction manifestation for YY-sites.

The performance of the 55 sites and effective stress analyses presented herein emphasize the need to consider system response of deposits when evaluating liquefaction and associated damage. In fact, they demonstrate governing influence of system response effects on liquefaction manifestation and emphasize the need to incorporate such considerations in the simplified liquefaction evaluation procedures, in which, currently, each layer is considered in isolation and system processes are not rigorously quantified. Clearly, a combination of factors is always at work, and further studies including detailed scrutiny of the NY sites are required to quantify some of the mechanisms elucidated in this study.

Acknowledgements

The first author would like to acknowledge the exceptional support provided by the Earthquake Commission New Zealand (EQC) to the geotechnical earthquake engineering research at the University of Canterbury over the past ten years. The '55 sites' project was funded by EQC. The second author would like to acknowledge the EQC Capability Funding Scholarship. The third author is a recipient of the EQC-QuakeCoRE scholarship. The '55 sites' project is a large collaborative effort including New Zealand and US researchers from the University of Canterbury, University of Auckland, Tonkin + Taylor, University of Texas, Austin, University of California, Berkeley, and University of California, Davis. This is QuakeCoRE publication number 0250.

References

[1] Biot MA. Theory of propagation of elastic waves in a fluid saturated porous solid, Part I—low frequency range; Part II—higher frequency range. J Acoust Soc Am 1956;28:168–91.
[2] Boulanger RW, Idriss IM. CPT and SPT based liquefaction triggering procedures. Report No. UCD/CGM-14/01. Davis: Center for Geotechnical Modeling, Department of Civil and Environmental Engineering, University of California; 2014.
[3] Cox BR, McLaughlin KA, van Ballegooy S, Cubrinovski M, Boulanger R, Wotherspoon L. In-situ investigation of false-positive liquefaction sites in Christchurch, New Zealand: St. Teresa's School case history. Vancouver, Canada: PBDIII Earthquake Geotechnical Engineering; 2017.
[4] Cubrinovski M, Ishihara K. Modelling of sand behaviour based on state concept. Soils Found 1998;38(3):115–27.
[5] Cubrinovski M, Ishihara K. State concept and modified elastoplasticity for sand modelling. Soils Found 1998;38(4):213–25.
[6] Cubrinovski M, Green RA, Allen J, Ashford S, Bowman E, Bradley B, Wotherspoon L. Geotechnical reconnaissance of the 2010 Darfield (Canterbury) earthquake. Bull NZ Soc Earthq Eng 2010;43(4):243–320.
[7] Cubrinovski M, Bradley B, Wotherspoon L, Green R, Bray J, Wood C, Wells D. Geotechnical aspects of the 22 February 2011 Christchurch earthquake. Bull NZ Soc Earthq Eng 2011;44(4):205–26.
[8] Cubrinovski M, Robinson K, Taylor M, Hughes M, Orense R. Lateral spreading and its impacts in urban areas in the 2010–2011 Christchurch earthquakes. NZ J Geol Geophys 2012;55(3):255–69.
[9] Cubrinovski M, Robinson K. Lateral spreading: evidence and interpretation from the 2010–2011 Christchurch earthquakes. Soil Dyn Earthq Eng 2016;91:187–201.
[10] Cubrinovski M, Rhodes A, Ntritsos N, van Ballegooy S. System response of liquefiable deposits. In: Proceedings of PBD III geotechnical earthquake engineering. Vancouver; July 2017.
[11] Darandeli MBG. Development of a new family of normalized modulus reduction and material damping curves [Ph.D. thesis]. Austin: University of Texas; 2001.
[12] Green RA, Cubrinovski M, Cox B, Wood C, Wotherspoon L, Bradley B, Maurer B. Select liquefaction case histories from the 2010–2011 Canterbury earthquake sequence. Earthq Spectra 2014;30(1):131–53.
[13] Idriss IM, Boulanger RW. Soil liquefaction during earthquakes. Monograph MNO-12. Oakland, CA: Earthquake Engineering Research Institute; 2008. p. 261.
[14] Iwasaki T, Tatsuoka F, Tokida K, Yasuda S. A practical method for assessing soil liquefaction potential based on case studies at various sites in Japan. In: Proceedings of the 2nd international conference on microzonation. National Science Foundation, Washington, DC; 1978.
[15] Maurer B, Green R, Cubrinovski M, Bradley B. Evaluation of the liquefaction potential index for assessing liquefaction hazard in Christchurch, New Zealand. J Geotech Geoenviron Eng, ASCE 2014;140(7). http://dx.doi.org/10.1061/(ASCE)GT.1943-5606.0001117.
[16] Moss RES, Seed RB, Kayen RE, Stewart JP, Der Kiureghian A, Cetin KO. CPT-based probabilistic and deterministic assessment of in situ seismic soil liquefaction potential. J Geotech Geoenviron Eng, ASCE 2006;132:1032–51.
[17] Rhodes A. Liquefaction evaluation in stratified soils [ME thesis]. Christchurch: University of Canterbury; 2017.
[18] Robertson PK, Wride CE. Evaluating cyclic liquefaction potential using cone penetration test. Can Geotech J 1998;35(3):442–59.
[19] Russell J, van Ballegooy S. Canterbury earthquake sequence: increased liquefaction vulnerability assessment methodology. T + T report prepared for the earthquake commission; 2015.
[20] Tsukamoto Y, Ishihara I, Nakazawa H, Kamada K, Huang Y. Resistance of partly saturated sand to liquefaction with reference to longitudinal and shear wave velocities. Soils Found 2002;42(6):93–104.
[21] Van Ballegooy S, Malan P, Lacrosse V. Liquefaction vulnerability study. T + T report prepared for the earthquake commission; 2013.
[22] Van Ballegooy S, Malan P, Lacrosse V, Jacka ME, Cubrinovski M, Bray JD, O'Rourke TD, Crawford SA, Cowan H. Assessment of liquefaction-induced land damage for residential Christchurch. Earthq Spectra 2014;30(1):31–55.
[23] Van Ballegooy S, Cox SC, Thurlow C, Rutter HK, Reynolds T, Harrington G, Smith T. Median water elevation in Christchurch and surrounding area after the 4 September 2010 Darfield Earthquake, Version 2. GNS Science Report 2014/18; 2014b.
[24] Yee E, Stewart JP, Tokimatsu K. Elastic and large-strain nonlinear seismic site response from analysis of vertical array recordings. J Geotech Geoenviron Eng 2013;139(10):1789–801.